



**HAL**  
open science

# Fe-doped olivine and char for in-bed elimination of gasification tars in an air-blown fluidised bed reactor coupled with oxidative hot gas filtration

Miguel Ruiz, Adam Schnitzer, Claire Courson, Guillain Mauviel

## ► To cite this version:

Miguel Ruiz, Adam Schnitzer, Claire Courson, Guillain Mauviel. Fe-doped olivine and char for in-bed elimination of gasification tars in an air-blown fluidised bed reactor coupled with oxidative hot gas filtration. *Carbon Resources Conversion*, 2022, 5 (4), pp.271-288. 10.1016/j.crcon.2022.07.004 . hal-03855345

**HAL Id: hal-03855345**

**<https://hal.science/hal-03855345>**

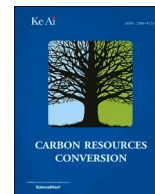
Submitted on 16 Nov 2022

**HAL** is a multi-disciplinary open access archive for the deposit and dissemination of scientific research documents, whether they are published or not. The documents may come from teaching and research institutions in France or abroad, or from public or private research centers.

L'archive ouverte pluridisciplinaire **HAL**, est destinée au dépôt et à la diffusion de documents scientifiques de niveau recherche, publiés ou non, émanant des établissements d'enseignement et de recherche français ou étrangers, des laboratoires publics ou privés.



Distributed under a Creative Commons Attribution - NonCommercial - NoDerivatives 4.0 International License



# Fe-doped olivine and char for in-bed elimination of gasification tars in an air-blown fluidised bed reactor coupled with oxidative hot gas filtration

Miguel Ruiz<sup>a,\*</sup>, Adam Schnitzer<sup>a,b</sup>, Claire Courson<sup>c</sup>, Guillain Mauviel<sup>a</sup>

<sup>a</sup> LRGP, CNRS, University of Lorraine, ENSIC, 1 Rue Grandville, Nancy, France

<sup>b</sup> University of Lorraine, LERMaB, ENSTIB, 27 Rue Philippe Séguin, PO Box 1041, F-88051 Epinal, France

<sup>c</sup> Institut of Chemistry and Processes for Energy, Environment and Health, ICPEES – UMR 7515, University of Strasbourg, 25 Rue Becquerel, 67087 Strasbourg, France

## ARTICLE INFO

### Keywords:

Gasification  
Tar  
Oxidative hot gas filtration  
Char  
Iron-doped olivine

## ABSTRACT

Gasification experiments were carried out in a pilot scale fluid bed reactor operated under allothermal mode and low fluidisation regime with iron-doped olivine and char as catalyst for in-situ tar abatement.

The catalyst combination resulted in a reduction of 50% in the overall tar yield with respect to the reference values. Furthermore, the integration of an oxidative Hot Gas Filtration unit downstream the gasification reactor led to a further reduction in overall tar yield and relatively clean gas was obtained (approx. 1 g/Nm<sup>3</sup>, benzene-free). The tar dew point of the resulting producer gas was estimated to 80 °C, only 40 °C above the threshold value recommended for its valorisation in standard internal combustion engines. Moreover, catalyst elutriation and char hold-up took place to a large extent inside the reactor. The analysis of catalyst samples at different Time-On-Stream (TOS) revealed: (i) a considerable loss of iron oxides during the first hour of test because of the interparticle mechanical attrition (mostly surface abrasion) and partial reduction of hematite to magnetite and wustite but, stable composition at higher TOS, (ii) the loss of the iron oxide coverage of Fe/olivine particles and the formation of agglomerates with increasing TOS and, (iii) the amount of carbon deposited in the surface of the Fe/olivine particles increased with TOS, but in any case, these carbon deposits can be completely oxidized above 650 °C.

## 1. Introduction

Gasification is a commercially available and flexible technology for the conversion of biomass residues and waste to a gas vector (syngas) with a high potential to substitute fossil-fuels in the production of heat, power, and chemicals. When air is employed as gasification agent, gasification reaction yields a N<sub>2</sub>-diluted syngas referred as producer gas. This latter typically contains pollutants, such as solids and tars, that restraint its end-user applications. For instance, tar concentration threshold value for internal combustion applications is typically reported within the range 10–100 mg/Nm<sup>3</sup> [1,2]. To address this issue, a lot of research has been conducted during the last decades on primary and secondary clean-up methods based on mechanical-physical, thermal and catalytic strategies [3,4]. For example, Kurkela et al. [5] reported tar content lower than 100 mg/Nm<sup>3</sup> during long term steam-oxygen gasification followed by downstream Hot Gas Filtration (HGF) and catalytic reforming with ZrO<sub>2</sub>, noble metal and nickel catalysts. Nevertheless, increasing complexity of the clean-up strategy negatively affects

the overall economy of the process. Ergo developing simple and inexpensive producer gas clean-up methods is necessary to foster the development of the gasification route.

Chars derived from pyrolysis and gasification units and some minerals, such as olivine and dolomite, are abundant and relative low-cost materials with a proven catalytic activity for the abatement of gasification tars at high temperature [6–9]. Substantial differences on mechanical properties (crushing and impact strength) between chars and minerals impose different reactor configuration for the use of these materials as catalysts at industrial scale.

On the one hand, chars are generally placed in fixed bed downstream the pyrolysis reaction stage. Some examples are the NoTar® gasifier [10], based on the downdraft configuration and, the decoupled two-stage configuration [11,12]. Another option is the integration of a Hot Gas Filter downstream the reactor stage. Thus, the fine char particles elutriated from the reactor are retained in the filter surface and forms the filter cake, promoting the contact between char particles and tars transported in the producer gas. Tuomi and co-workers [13] reported a

\* Corresponding author.

E-mail address: [miguel.ruiz@keemail.me](mailto:miguel.ruiz@keemail.me) (M. Ruiz).

<https://doi.org/10.1016/j.crcon.2022.07.004>

Received 16 February 2022; Received in revised form 9 July 2022; Accepted 17 July 2022

Available online 20 July 2022

2588-9133/© 2022 The Authors. Publishing services by Elsevier B.V. on behalf of KeAi Communications Co. Ltd. This is an open access article under the CC BY-NC-ND license (<http://creativecommons.org/licenses/by-nc-nd/4.0/>).

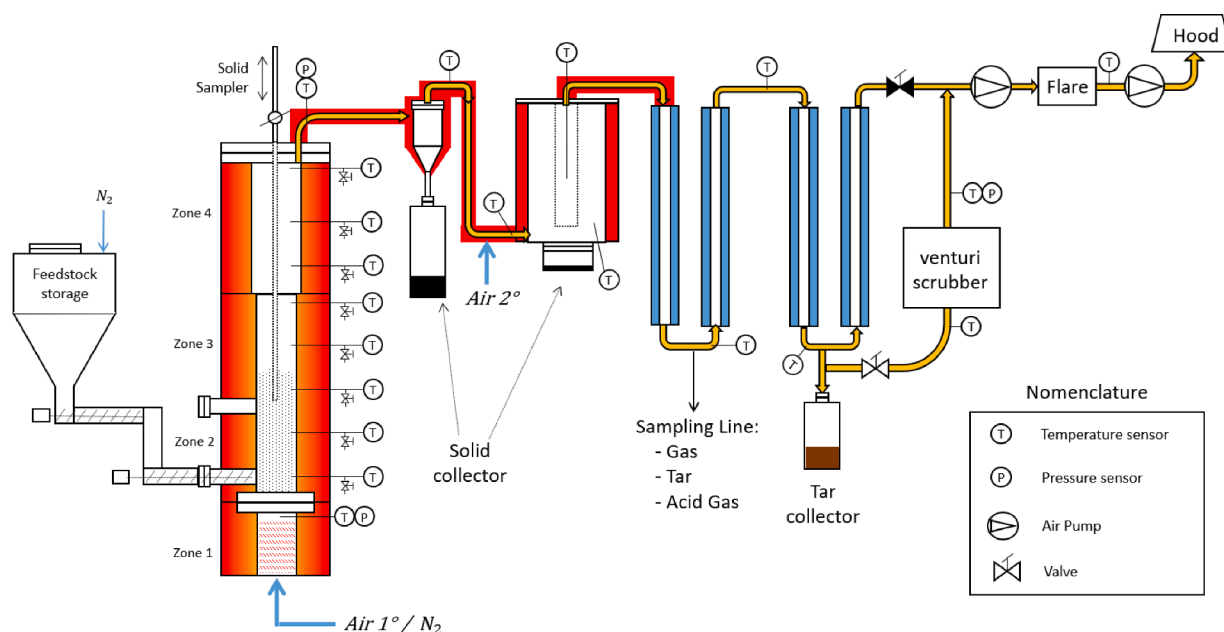


Fig. 1. Schematic view of the gasification rig under the HGF configuration.

tar removal efficiency about 50 % during steam gasification tests with dolomite as bed material and a HGF kept at 800 °C. Moreover, other authors have reported steady operation of the HGF unit for over 200 h [14] and significative tar removal efficiencies by injecting a small amount of secondary air into the HGF unit kept under mild hot temperature conditions (400–600 °C) [15].

On the other hand, minerals, such as olivine and dolomite, are typically used in simple and circulating fluidized bed configurations. Compared to dolomite, olivine offers the advantage of attrition resistance resulting in lower content of solid particles in the producer gas [6,16]. Several methods have been studied to improve the attrition resistance and catalytic activity of olivine grains, such as thermal treatment and metal-doping.

Thermal treatment (calcination) at high temperatures (greater than 900 °C) is known to produce phase transformation and migration of iron from the inner part of olivine grains towards the surface [18–21], impacting positively the attrition resistance, as well as improving the tar abatement activity of olivine grains [17,22].

Metal-doping of olivine grains with costly metals, i.e. nickel, has shown to increase the catalytic activity for tar abatement [23–25], but its relatively high cost and toxicity hinder to some extent its utilisation at industrial scale. By contrast, iron and iron oxides are naturally abundant, inexpensive and non-toxic materials with a proven catalytic activity in the conversion of tar [26–31] and tar surrogates [20,32,33]. Fredriksson et al. [34] pointed out the influence of simulated oxidizing/reducing gas environments on the chemical state of Fe-phases and iron oxides and its amount on the surface of olivine. Authors reported that after exposure to reducing gases (H<sub>2</sub>, CO), the iron oxides are converted to Fe<sup>0</sup> and Fe<sub>3</sub>C and formation of graphitic carbon is observed whereas, after the exposure to oxidizing gases (O<sub>2</sub>, H<sub>2</sub>O, CO<sub>2</sub>), the free phases are (Fe<sub>2</sub>O<sub>3</sub>, Fe<sub>3</sub>O<sub>4</sub> or MgFe<sub>2</sub>O<sub>3</sub>). Moreover, the redox properties of iron and iron oxides inherently present or added to olivine grains has attracted much attention for its application in circulating bed systems where olivine grains act as oxygen carrier between the combustion and reformer reactor. For example, Virginie et al. [35] reported a 65 % drop on the tar concentration when iron-doped olivine was used instead of olivine during steam gasification in a dual fluidized bed reactor system. Extensive characterisation of used catalyst confirmed: (i) stable structure after many oxidizing-reducing cycles and, (ii) coke deposited in catalyst surface was easily oxidized. Pan et al. [36] reported a 80 % drop

in the tar concentration during the co-gasification of biomass and coal in a decoupled triple bed with Fe<sub>2</sub>O<sub>3</sub>/olivine catalyst compared to quartz. Nevertheless, the tendency of iron oxides to attrit when exposed to high mechanical and thermal stresses created inside circulating bed systems [37], make necessary a continuous back-up of the catalytic material compromising the economic performance of the process face to currently available methods for tar elimination, i.e. wet scrubbing.

In-bed elimination of tars by in-situ produced char has been recently pointed out by Tsuboi and co-workers [38] as a simple strategy to promote tar decomposition while keeping the system configuration as simple as possible. Indeed, it is well known that the degree of char conversion in fluidized beds is strongly influenced by the degree of fuel mixing (in lateral and axial directions), which in turns is determined, *inter alia*, by the superficial velocity of the gas, the fuel properties and the topology of the reactor [39–41]. Therefore, by operating the reactor at slow fluidisation regime (in [38] the ratio of the gas velocity (U<sub>0</sub>) to the minimum fluidisation velocity (U<sub>mf</sub>) was kept about 1.5), the segregation of char particles at the upper part of the reactor was promoted providing a char-rich bed for tar decomposition. However, the effect of the char-rich bed on tar content and composition was not addressed.

The purpose of this study is to explore the synergies of char hold-up and iron-doped olivine for the in-bed elimination of gasification tars in a fluidized bed reactor operated under low fluidisation regime and coupled with an oxidative HGF unit. Additionally, the effects of time-on-stream (TOS) on catalyst properties were assessed by comprehensive catalyst characterisation (structure, iron oxide reducibility, morphology, and carbon deposition) before and after gasification.

## 2. Materials and methods

### 2.1. Feedstock, gasification rig and analytical methods

Gasification tests were conducted in a pilot scale 1–10 kg/h fluidized bed reactor fully detailed elsewhere [15]. Briefly, pellets of *N*-rich Medium-Density Fibreboard (MDF) were continuously injected at the bottom of the reactor by a double screw system and gasified using air. Results of elemental and proximate analyses of MDF were included in table B.4 (Annex B). The reactor was externally heated and operated under allothermal mode at constant temperature. A cyclone separator,

**Table 1**  
System configuration, nomenclature, and target conditions for all experiments.

System configuration	Test code	Bed material	ER <sub>HGF</sub>	ER <sub>total</sub>	Test duration (h)	Catalyst TOS (h)
<b>Cyclone</b>	REF (x2)	Olivine	0	0.25	2	2
	Fe/Oliv-1 h	Fe/olivine	0	0.25	1	1
	Fe/Oliv-2 h	Fe/olivine	0	0.25	2	2
	Fe/Oliv-4 h	Fe/olivine	0	0.25	4	4
<b>Cyclone + HGF</b>	Fe/Oliv HGF-1	Fe/olivine	0.05	0.3	4	4
	Fe/Oliv HGF-2	Fe/olivine*	0.05	0.3	4	8

\*Fe/olivine material recovered after the test Fe/oliv HGF-1 was reused for the test Fe/oliv HGF-2.

placed downstream of the gasification reactor, was employed to remove the coarse particles elutriated from the fluidized bed. Next, the producer gas was cooled down in three heat exchangers before it enters the wet scrubber operated with water. Finally, the gas was flared to avoid safety issues. To carry out the HGF tests, a HGF unit was installed downstream the cyclone separator and kept at temperature of 450 °C by external heating to avoid tar condensation. Multilayer metallic filtration cartridges, provided by GKD [42], were used as filtration media. Filtration cartridges consisted of an outer thin metal fabric with a mean pore size of 10 µm followed by a 2–3 mm layer of non-woven metal fibres supported on a metallic frame. A schematic view of the gasification rig under the HGF configuration is detailed in Fig. 1. Filter cake oxidation was accomplished by the injection of a flow of secondary air into the HGF and no back-pulse system was employed in any of the filtration tests. The main operational parameters of the HGF unit were detailed in Table 2.

Permanent gases and tars contained in the producer gas were sampled at the exit of the first heat exchanger following a modified version of the tar protocol and analysed by complementary analytical techniques, such as: µ-GC, HPLC-UV, GC-MS/FID and Synchronous Fluorescence Spectroscopy (SFS). Moreover, since MDF typically presents a high content in Fuel Bounded Nitrogen (FBN), inorganic gases (NH<sub>3</sub> and HCN) were quenched separately in two impinger trains and quantified by ion chromatography. Surface observation and analysis of the filter mesh was conducted with a Scanning Electron Microscope (SEM) coupled with Energy Dispersive X-ray (EDX) (JEOL JSM6490 LV). A full description of all analytical methods can be found elsewhere [15].

## 2.2. Catalyst preparation and characterization

Non-doped olivine (further referred as olivine) was provided by Magnolithe GmbH Austria [43] with a particle size distribution between 0.3 and 0.4 mm and a mean diameter of 387 µm (see Fig. A1, appendix A). To increase its mechanical resistance, providers applied a calcination at 1600 °C for 4 h. Results of the characterisation of this commercial material have been already reported by Virgine et al. [35] indicating a chemical composition (wt%) of 30.5 Mg-19.6Si-7.1Fe. Moreover, authors indicated that half of the 7.1 wt% Fe is present as Fe(III) oxides (α-Fe<sub>2</sub>O<sub>3</sub>, MgFe<sub>2</sub>O<sub>4</sub>) and the other part is present as Fe(II) inside the olivine structure.

Fe-doped olivine (further referred as Fe/Olivine) was synthesized

from Magnolithe® (original particle size of 0.2–0.3 mm) by wet impregnation followed by drying and calcination at 1000 °C for 4 h. The preparation protocol is fully described elsewhere [35]. Results of ICP-MS measurement reported previously [35] indicated a total iron content in the Fe/olivine of approximately 16 wt% after the impregnation protocol. Particle size distribution of synthesized particles of Fe/olivine was adjusted to 0.3–0.8 mm by sieving. Mean particle size after sieving was equal to 382 µm (see Fig. A1, appendix A).

As a result of the synthesis method used in this study, the calcination temperature after Fe impregnation was reduced to 1000 °C. Latter value is significantly lower compared to the temperature required with mechanical mixture (at least 1400 °C) to create interaction between olivine and added iron [44]. These interactions appeared as spinel phase (MgFe<sub>2</sub>O<sub>4</sub>) and Liebenbergite phase (Ni<sub>2</sub>SiO<sub>4</sub>) but no nickel nor iron oxide was observed.

X-ray diffraction was conducted to obtain structural information about the crystallinity of the catalyst. XRD spectra were taken using a Bruckner AXS D8 Advanced powder spectrometer using CuK<sub>α</sub> radiation. The Bragg angle was 2θ = 20°–70° with a scanning step = 0.0158° and a sampling time = 1 s per step. Crystalline phases were then identified by Powder Diffraction Files (PDF) of International Centre of Diffraction Data (ICDD).

The reduction temperature and the reducibility of the catalyst was assessed using a Temperature Programmed Reduction (TPR) analysis. Powdery samples (100 mg), placed in a quartz packed bed reactor, underwent TPR managed by a Micromeritics Autochem II. TPR included a 15 °C.min<sup>-1</sup> heating up to 1000 °C under a reducing flowrate of 50 Nml.min<sup>-1</sup> (10 vol% of H<sub>2</sub> in Ar). Afterwards, the sample was cooled to room temperature under Ar flow. The hydrogen consumption was measured by a thermal conductivity detector (TCD) until the signal returns to the baseline.

The surface morphology of the catalyst samples was analysed using Scanning Electron Microscopy (SEM). Few grains of sample are sticking on a cylindrical dural sample carrier using double-sided adhesive tape. Pictures was taken by a Zeiss Gemini SEM 500 equipped with an In-lens SE detector, an electron high tension usually at EHT = 2 kV, a sample-objective distance of WD = 11–12 mm and different field width values indicating superficial composition and olivine covering by iron oxide.

Temperature Programmed Oxidation (TPO) was used to evaluate the carbon deposited on the sample by the incomplete oxidation of biomass compounds. Powdery samples (400 mg), placed in a quartz packed bed reactor, underwent TPO managed by a Micromeritics Autochem II. Each sample was firstly degassed and cleaned from physisorbed hydrocarbons, by a 30 °C.min<sup>-1</sup> heating ramp up to 700 °C and a cooling down to room temperature, all under a 50 Nml.min<sup>-1</sup> He stream. Actual TPO followed, including a 30 °C.min<sup>-1</sup> heating up to 900 °C under an air flowrate of 30 Nml.min<sup>-1</sup>. Afterwards, the sample was cooled to room temperature under He flow. The gas flow was analysed by thermal conductivity detector (TCD) to quantify the moles of CO and CO<sub>2</sub> formed during oxidation that correspond to the moles of C on the sample.

## 2.3. Experimental plan

Table 1 summarises the system configuration, test nomenclature and target conditions for all experiments conducted in this study. Six experimental runs were carried out under two system configurations corresponding to: (i) the standard cyclone configuration and, (ii) the cyclone + HGF configuration. Based on the system configuration and the experimental purpose of each experiment, the six runs were classified in three series explained below.

The first series correspond with two reference tests conducted under the cyclone configuration and with non-doped Olivine as fluidized bed material. The purpose of these tests was to establish a reference value for gasification indicators and tars with non-doped Olivine. Operational parameters inside the gasification reactor, namely: the primary air flow rate, the reactor wall temperature, the primary air-to-feedstock



**Table 2**

Main operation conditions, gasification indicators and product yields for all tests (individual yields of quantified tar molecules were detailed in Table B.1, Appendix B).

REF	Fe/ oliv-1 h	Fe/ oliv-2 h	Fe/ oliv-4 h	Fe/oliv + HGF- 1	Fe/oliv + HGF- 2	
<i>Gasifier</i>						
Bed temperature, °C	793 ± 1	791	790	799	796	797
Freeboard temperature, °C	763 ± 1	763	760	764	763	764
Char hold-up, g	293 ± 15	260	640	806	793	910
Recovered olivine, kg	3.89 ± 0.15	2.60	2.76	3.13	3.06	2.72
Purge-N <sub>2</sub> in feeding system, NL/h	1099	1099	1099	550	550	550
U/U <sub>mf</sub>	2.7	2.7	2.6	2.7	2.6	2.6
ER <sub>reactor</sub>	0.24 ± 0.01	0.24	0.25	0.24	0.25	0.25
<i>Hot Gas Filtration Unit</i>						
Gas mixing zone temperature, °C	–	–	–	–	382	392
Filter temperature, °C (dirty side)	–	–	–	–	386	390
Filter temperature, °C (clean side)	–	–	–	–	467	484
Face filtration velocity, cm/s	–	–	–	–	1.24	1.21
Gas residence time inside HGF unit, s	–	–	–	–	27.6	28.1
ER <sub>HGF</sub>	–	–	–	–	0.05	0.05
ER <sub>total</sub>	0.24 ± 0.01	0.24	0.25	0.24	0.30	0.30
<i>Gasification output indicators<sup>d</sup></i>						
Gas Yield, Nm <sup>3</sup> /kg <sub>feed</sub> (daf)	1.58 ± 0.04	1.56	1.56	1.58	1.84	1.92
LHV, MJ/Nm <sup>3</sup>	5.3 ± 0.2	4.7	4.6	4.9	4.3	4.9
%CGE	45.5 ± 0.03	39.6	39.7	42.3	43.6	51.0
%C	55.3 ± 0.02	47.5	48.1	49.5	54.4	61.4
%H	50.0 ± 0.03	47.0	46.8	51.9	52.0	59.5
<i>Tar yield<sup>e</sup>, g/kg<sub>feed</sub> (daf)</i>						
benzene	6.4 ± 0.1	6.1	4.6	4.6	5.0	5.1
Class II - (heterocyclic)	0.44 ± 0.02	0	0.07	0.08	0.05	0.06
Class III - (Light aromatics)	4.56 ± 0.02	2.34	2.13	2.32	1.43	1.48
Class IV - (Light PAH)	3.55 ± 0.07	1.95	1.66	1.69	0.77	0.85
Class V - (heavy PAH)	0.20 ± 0.03	0.10	0.08	0.08	0.03	0.03
Total <sup>b</sup>	8.7 ± 0.1	4.4	3.9	4.2	2.3	2.4
Gas dew point <sup>c</sup> , °C	139 ± 2	130	124	112	80	83
Volume gas sampled tar protocol, NL	60	33.5	56.4	53.4	58.2	57.5
<i>Water and gas yield, g/kg<sub>feed</sub> (daf)</i>						
NH <sub>3</sub>	21.6 ± 1.7	–	17.9	–	–	20.2
HCN	1.3 ± 0.1	–	0.8	–	–	0.8
H <sub>2</sub> O	350 ± 11	370	331	315	315	290

<sup>a</sup> Tar groups according to the ECN tar classification. <sup>b</sup>Total tar yield is expressed on benzene-free basis. <sup>c</sup>Calculated using the complete model

developed by ECN (<https://www.thersites.nl>). dGasification output indicators were calculated excluding the flow of purge-N<sub>2</sub> injected into the feeding system.

equivalence ratio (ER) and the feedstock throughput, were kept constant at a value of 2330 NL/h, 800 °C, 0.25 and 2.4 kg/h (as received), respectively. For each test, a batch of 4 kg of fresh Olivine was loaded into the reactor and then, heated under air at 800 °C for 1 h before the injection of the feedstock. Fluidisation velocity (U<sub>0</sub>), calculated on the empty-bed basis, was 2–3 times greater than the minimal fluidisation velocity (U<sub>mf</sub>) equals to 0.11 m/s at 800 °C (as measured in this set-up). Under these conditions, gas residence time inside the reactor was 8 s. Results reported corresponds with the average and standard deviation values calculated from the two repeated tests (hereafter named as REF).

The second series gather three tests, namely Fe/Oliv-1 h, Fe/Oliv-2 h and Fe/oliv-4 h, conducted under the cyclone configuration and identical operational conditions as for the reference tests, but with Fe/Olivine instead of Olivine and a duration of 1, 2 and 4 h, respectively. The objective of this series was twofold: (i) to assess the combined effect of char hold-up and Fe-doped Olivine on the output indicators and products yields and, (ii) to study the impact of catalyst time-on-stream (TOS) on the properties of iron-doped Olivine. For each test, a batch of 4 kg of fresh Fe/Olivine was loaded into the reactor and then, heated under air at 800 °C for 1 h before the injection of the feedstock. The U<sub>mf</sub> of the Fe/olivine was identical as for the non-doped olivine even though the former presented a slightly different hydrodynamic behaviour. Indeed, the wider size distribution of the raw Fe/olivine particles (see Fig. A.1 and A.2, Appendix A) led to the formation of a semi-fluidised region in the process of fluidization. However, the expected increase in the value of U<sub>mf</sub> was offset as a result of lubricating effects induced by the presence of particles of different size [45].

For the third series, the HGF unit was installed downstream the cyclone separator and two consecutive tests, namely Fe/Oliv HGF-1 and Fe/Oliv HGF-2, were conducted using a unique batch of 4 kg of Fe/Olivine. During the test Fe/Oliv HGF-2, de-fluidisation issues inside the reactor may happen if excessive char hold-up exists. Therefore, the bed inventory (composed of used Fe/Olivine and char) was recovered after the test Fe/Oliv HGF-1 and the Fe/Olivine was separated from the char by manual sieving. Then, the separated Fe/Olivine was reloaded into the reactor for the test Fe/Oliv HGF-2. Therefore, in terms of TOS, the batch of Fe/Olivine recovered after the test Fe/Oliv HGF-2 accumulated 8 h of exposition under real gasification environment. Moreover, a small flow of air (420 NL/h) was continuously injected in the HGF unit during both tests to oxidize the carbon-rich dust particles deposited on the filter surface. Finally, the filter cake accumulated on the surface of the HGF cartridges was not removed between the two consecutive tests.

For all the experimental runs conducted in this study, tar and acid gas sampling were systematically performed during the last 40 min of each test. Moreover, to avoid the combustion of the remaining carbon-rich particles inside the reactor and HGF unit at the end of the tests, as well as to stop further evolution of the catalyst properties, an inertization procedure was set-up. Briefly, shortly after shutdown the biomass feeding, the fluidising agent (air) was switched to N<sub>2</sub> (0.5 Nm<sup>3</sup>/h) until the system temperature inside the reactor was below 70 °C. Once the reactor was cooled, the bed inventory (composed of Olivine and char) was recovered by vacuum aspiration. Then, the char was separated from Olivine by manual sieving. The “char hold-up” and the “recovered Olivine” correspond with the mass of char and Olivine weighted after separation.

The performance of the gasification process was assessed using four output indicators, namely Low Heating Value (LHV), Gas yield ( $\eta_{\text{gas}}$ ), Cold Gas Efficiency (CGE) and Carbon Conversion (%C), fully described elsewhere [15], and calculated excluding the benzene of the composition of the producer gas. Moreover, to avoid misinterpretation the gasification output indicators were calculated excluding the flow of N<sub>2</sub> injected into the feeding system for purge and pressure stabilisation

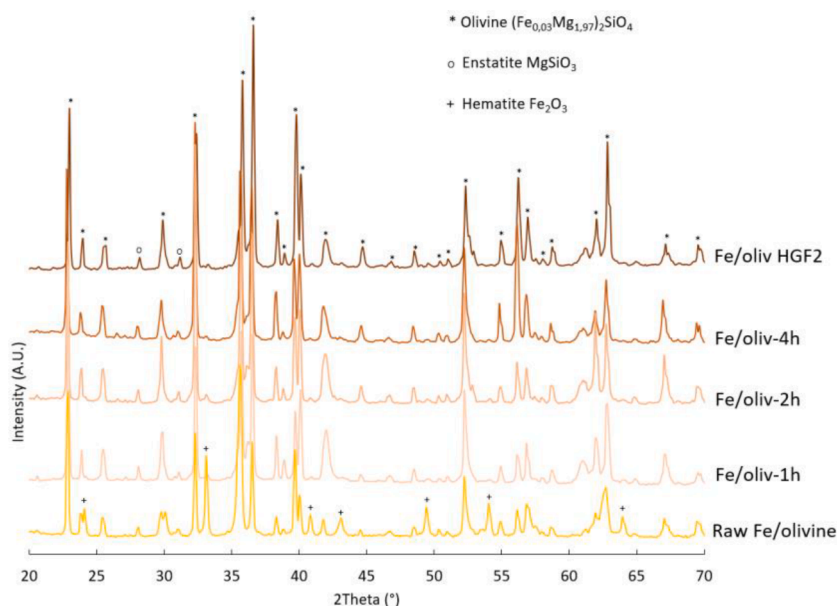


Fig. 2. Diffractograms of fresh and used iron-doped olivine samples

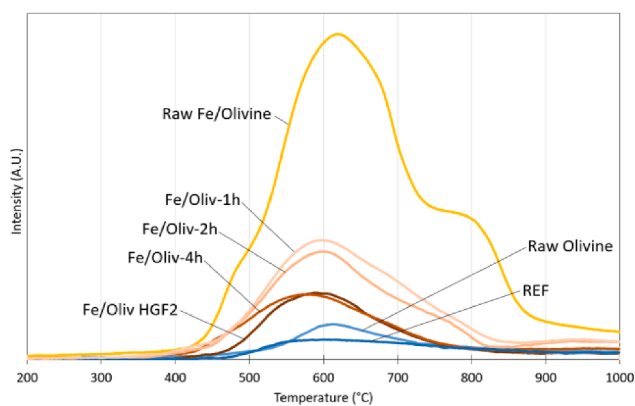


Fig. 3. Profiles of H<sub>2</sub> consumption of fresh and used catalyst samples.

purposes. Finally, the conversion percentage was calculated according to Equation (1), using the average value determined for the three reference tests as reference value.

$$Conversion, \% = \frac{(\gamma_i - \gamma_{REF}) * 100\%}{\gamma_{REF}} \quad (1)$$

where  $\gamma$  represents the yield value of each group or molecule in g/kg<sub>feed</sub> daf.

### 3. Results and discussion

#### 3.1. System operation

The temperatures in the dense-bed and freeboard zones of the gasification reactor were roughly identical in all tests and equals to 800 °C and 760 °C, respectively (see Table 2). For the two HGF experiments (Fe/Oliv HGF-1 and Fe/Oliv HGF-2), the gap of 80–90 °C between the temperature of the dirty and clean side of the filter resulted from the partial oxidation of carbon-rich particles deposited on the filter surface [15].

The masses of the bed inventory recovered after each test (see Table 2) indicated the occurrence of two opposite phenomena: (i) the elutriation of olivine particles from the reactor, particularly for the tests conducted with iron-doped olivine and, (ii) the accumulation of char

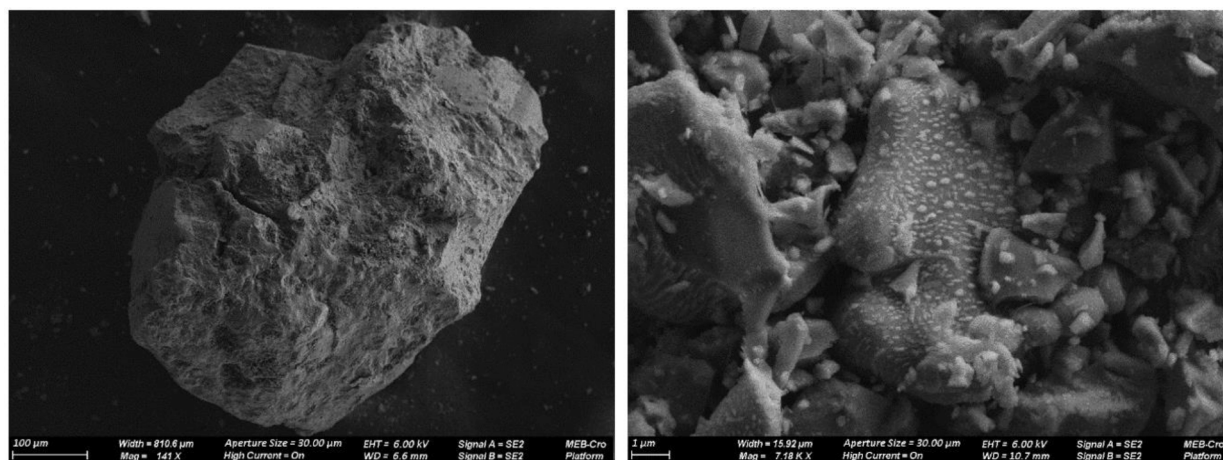


Fig. 4. SEM images of fresh Olivine.



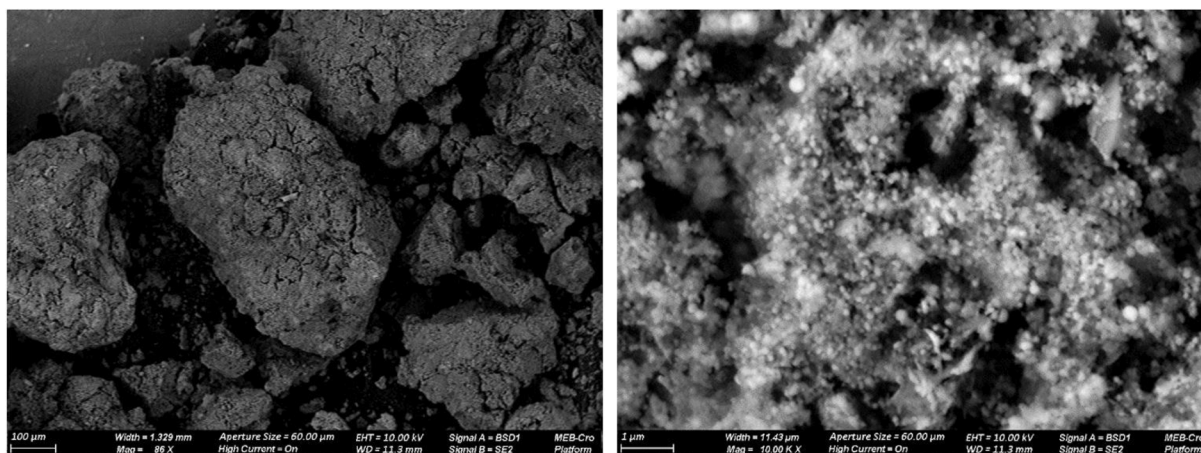


Fig. 5. SEM images of fresh Fe/Olivine.

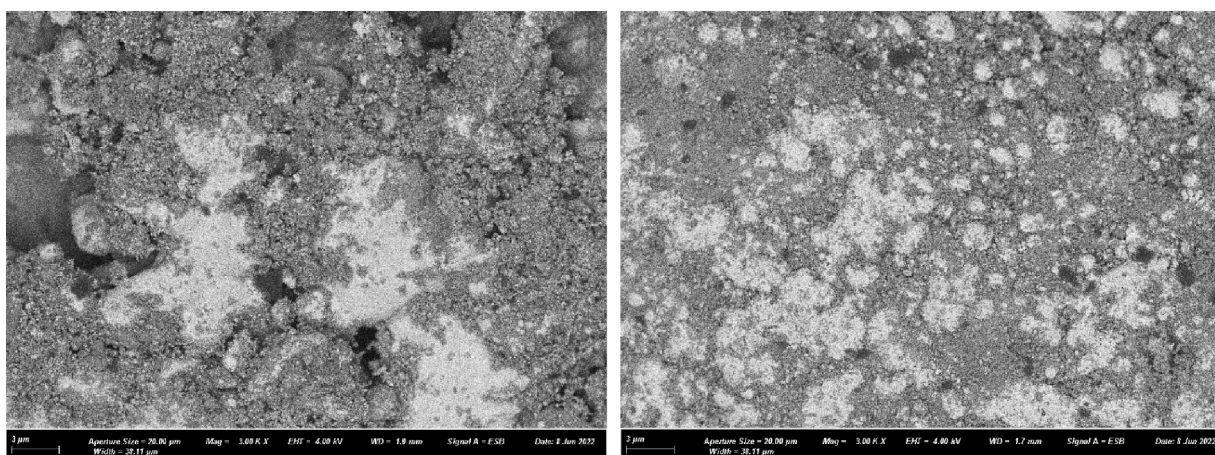


Fig. 6. SEM images of Fe/Oliv-1 h (left) and Fe/Oliv-2 h (right).

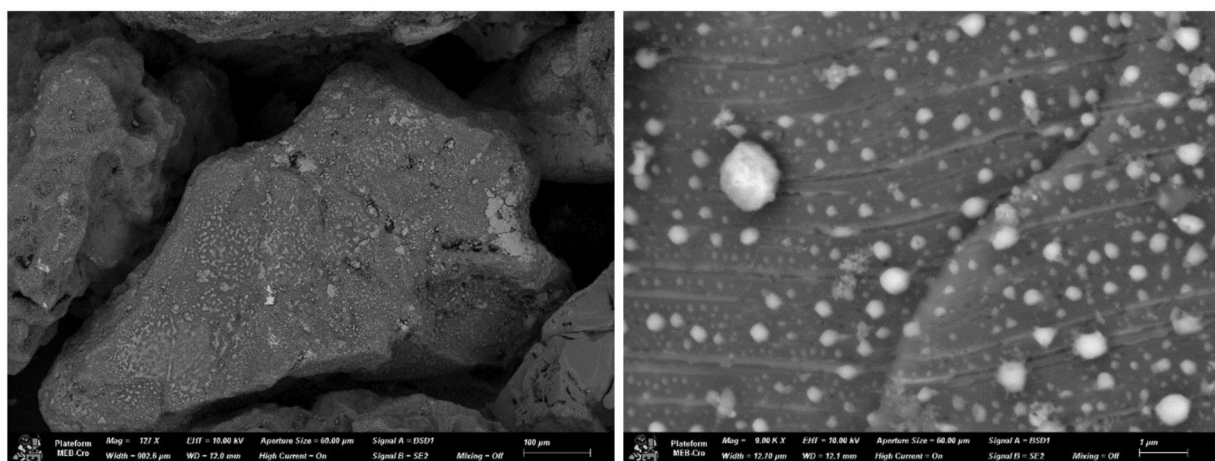


Fig. 7. SEM images of Fe/Oliv-4 h.

inside the reactor. Because of their relevance, these two phenomena are discussed in the paragraphs below.

On the one hand, the mass values of recovered olivine catalyst confirmed a more severe elutriation for the tests conducted with iron-doped olivine than for the tests conducted with non-doped olivine. In the latter case only 5 % of the olivine was elutriated. Indeed, the narrow

size distribution of olivine grains (0.2–0.3 mm) used to prepare the Fe/Olivine catalyst was widened and shifted to higher values during the synthesis procedure because of the surface deposition of iron oxide and the interparticle aggregation (see Fig. A.1, Appendix A). Then, the high interparticle mechanical attrition occurring within the dense bed, mostly controlled by surface abrasion [37], caused the wearing of

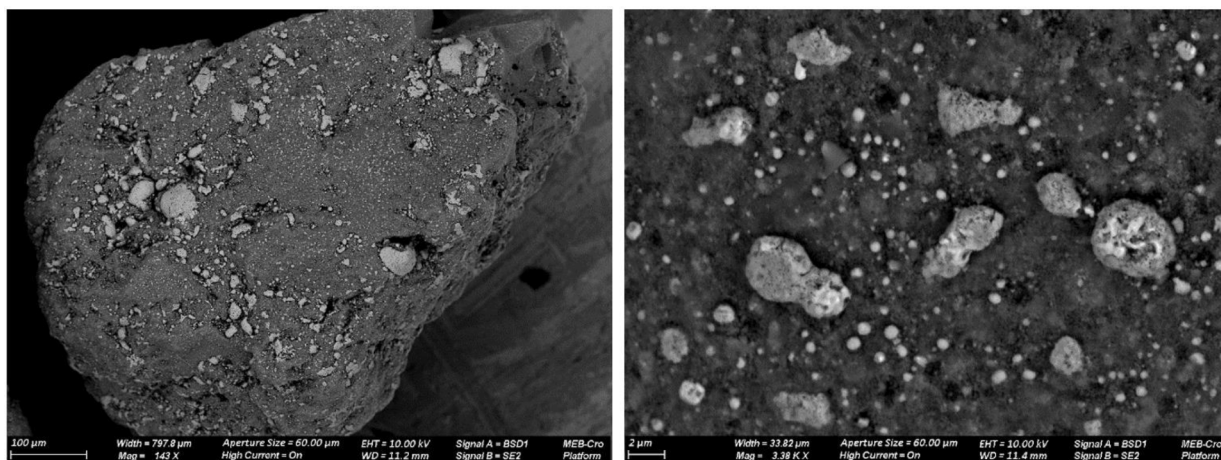


Fig. 8. SEM images of Fe/Oliv HGF-2.

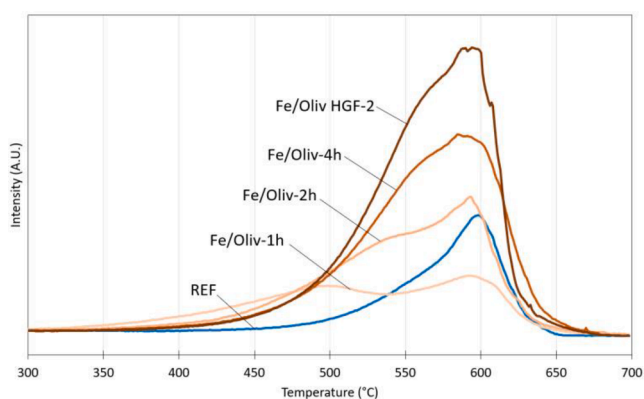


Fig. 9. TPO (Temperature Programmed Oxidation) of used olivine catalyst samples.

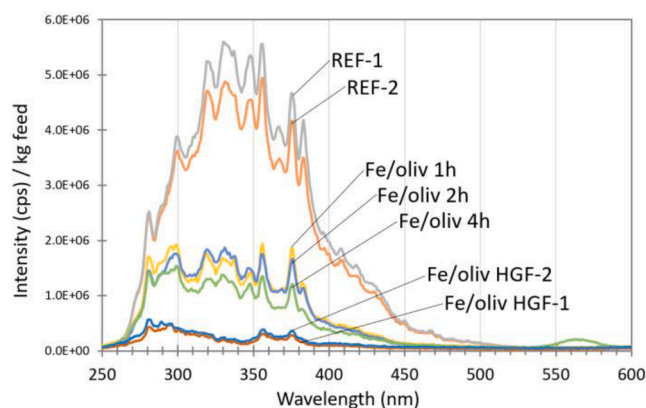


Fig. 11. Synchronous Fluorescence spectra recorded at offset = 20 nm of tar protocol samples.

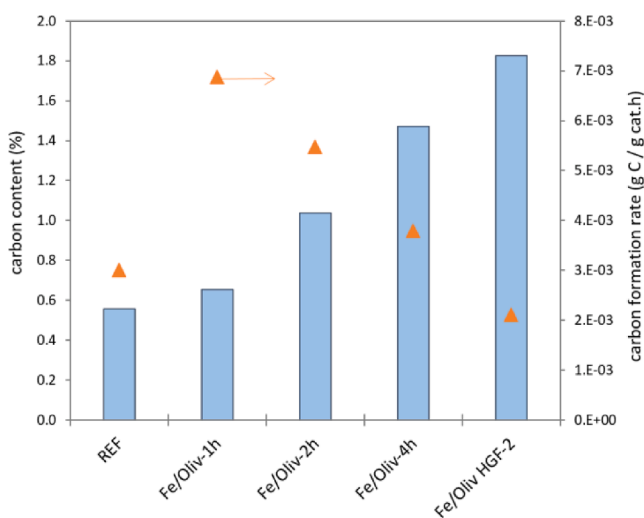


Fig. 10. Amount of carbon deposited on each sample and carbon formation rate during gasification tests at different TOS.

surface iron oxides and the separation of the agglomerates, increasing the small particle size fraction of the Fe/Olivine inventory (see Fig. A.2, Appendix A). Consequently, the mass of Fe/Olivine catalyst elutriated from the reactor during the tests Fe/Oliv-1 h and Fe/Oliv-2 h was very high (30–35 % of the initial mass of catalyst). It was then decided to reduce the flowrate of purge-N<sub>2</sub> by a half after the installation of a small heat exchanger on the second feeding screw. By doing that, the percentage of Fe/Olivine elutriated was reduced to 20–25 % at the end of the tests Fe/Oliv-4 h and Fe/Oliv HGF-1. By contrast, the mass of Fe/Olivine elutriated for test Fe/Oliv HGF-2 represented only 11 % of the initial load, which seems logical if we consider that the catalyst was already used for the test Fe/Oliv HGF-1. Latter value was only 5 % higher than the percentage of Olivine elutriated during the REF tests.

On the other hand, char hold-up values showed a clear correlation with the duration of the test. For all tests, char particles recovered from the reactor presented a wide size distribution between 1.5 and 4.2 mm and a mean diameter equals to 2054 μm. As expected, the low fluidization regime in the gasification reactor ( $U_0/U_m \approx 2-3$ ) reduced the degree of char conversion increasing the char hold-up inside the reactor. According to [39], the low degree of char conversion was likely linked to: (i) the poor lateral and axial mixing of char and olivine and, (ii) the lower attrition and elutriation of char particles. Furthermore,



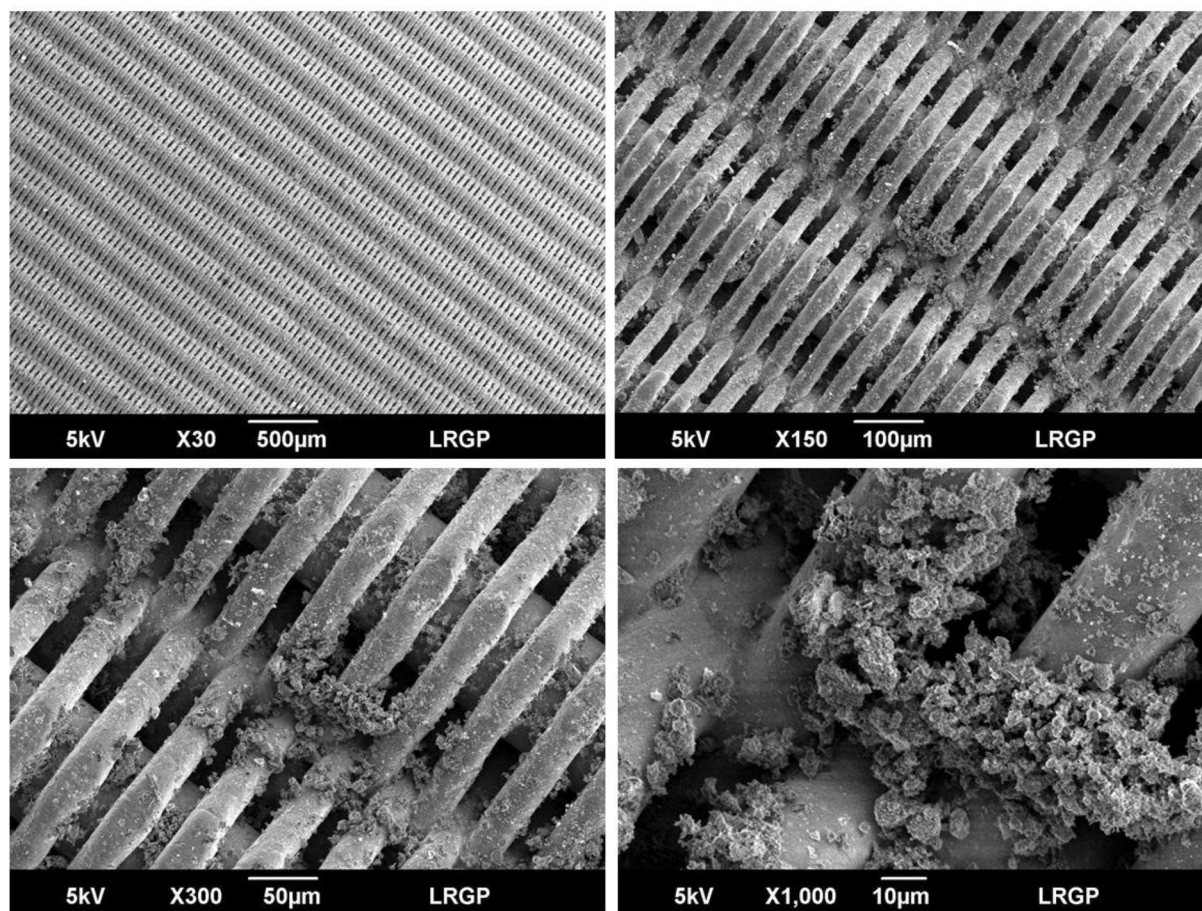


Fig. 12. SEM images of the surface (dirty side) of the metallic filter cartridge after the test Fe/oliv-HGF-2.

stabilization of the pressure drop across the reactor after 3 h (observed for the tests with a duration of 4 h), indicated a reduction in the char accumulation inside the reactor (see Fig. A.3, Appendix A).

Finally, to illustrate the impact of olivine elutriation and char hold-up on the structure of the dense bed inside the reactor, the bed material inventories recovered after each test were poured in a transparent cylinder at ambient temperature (Fig. A.4, Appendix A). These results showed that for the tests with a duration of 4 h, approximately the half of the reactor was occupied by the bed material (olivine and char). Indeed, the configuration chosen for the representation of the bed inventory (olivine particles at the bottom and the char particles at the upper part of the reactor) is only indicative because no measure of the particle mixing degree within the dense bed was carried out during the tests. According to the general fluidisation rules proposed by Chiba et al. [46] for binary mixtures of solids, when the size ratio between the bigger and smaller component is below 10, the heavier component sinks (jetsam) and the bigger component floats (flotsam). In this study, the size ratio (based on mean particle size) between the char and the Olivine particles of the bed inventory was equal to 5. Therefore, it is likely that most of the olivine remained at the bottom of the reactor. Latter consideration is supported by the axial composition of the bed inventory determined by Lardier et al. [47] using the same gasification reactor but, feeding the biomass pellets at the top of the reactor. Additional measures would be necessary to determine the hydrodynamic behaviour of the dense bed and the axial gas composition profile inside a gasification reactor operated under a low fluidization regime at high temperatures.

### 3.2. Catalyst characterisation

X-ray diffractograms, depicted in Fig. 2, indicated that Olivine structure was maintained in all samples after test. Iron oxide ( $\text{Fe}_2\text{O}_3$ ), added by impregnation of iron nitrate on Olivine and calcination, was detected in the fresh catalyst (raw Fe/Olivine). The intensity of the rays corresponding to  $\text{Fe}_2\text{O}_3$  (hematite) dropped during the first hour of gasification and then remained at a constant level for all the other used samples of iron-doped catalyst (Fe/Oliv-1 h, Fe/Oliv-2 h, Fe/Oliv-4 h and Fe/Oliv HGF-2). The drop in the content of hematite can be explained by: (i) the attrition (surface abrasion) of Fe/Olivine grains which seems largely limited after 1 h of TOS and/or, (ii) by a partial reduction of hematite into magnetite ( $\text{Fe}_3\text{O}_4$ ) and wustite ( $\text{FeO}$ ) phases. In fact, these reduced phase of iron oxide were difficult to observe since their main rays are hidden by the multiple rays of the very well crystallized olivine structure. A very slight shift in the olivine rays was also observed for Fe/Oliv HGF-2, which may be associated with a greater amount of iron in the olivine structure due to iron mobility under reductive atmosphere as previously reported [29] and, with the lower intensity of iron oxide rays. Furthermore, no carbon was detected by XRD on the used catalyst samples whatever the TOS.

It appears from the TPR results, showed in Fig. 3, that the fresh catalyst (Raw Fe/Olivine) contains a large amount of reducible iron oxide. This phase will be reduced into  $\text{Fe}_3\text{O}_4$ ,  $\text{FeO}$  and metallic iron because its reduction temperature is compatible with the gasification one. Then the Fe/olivine will be activated *in situ*. As expected, after 1 h



of gasification, this amount is greatly reduced (divided by more than 2) by partial reduction of iron oxides and/or attrition. Moreover, the amount of reducible iron oxide continues to decrease with an increase in TOS to stabilize between 4 h and 8 h at a value twice as high as the fresh non-doped olivine used for the synthesis of the iron-doped catalyst. Furthermore, the decrease in the intensity of the TPR profile observed between the non-doped fresh (raw olivine) and used (REF) olivine was probably linked to the attrition of the grains and/or to the reinsertion of iron in the olivine structure under reductive conditions of gasification as observed by XRD and previously reported [21].

The loss of reducible iron should lead to a deactivation of the catalyst versus TOS. It was then important to check the covering of olivine grains by iron oxide after tests with various TOS and to study its morphology evolution by SEM and EDX analysis.

**Fresh olivine:** The morphology of fresh non-doped olivine particles, showed in Fig. 4, consists in the sum of angular small fragments due to the preliminary calcination at 1600 °C and the grinding / sieving to obtain the desired particle size. On the surface of the olivine, very well crystallized iron oxides crystals (white because analyzed by a back-scattered electron detector) appear to be aligned on parallel axes. The EDX analysis (Fig. A.5, Appendix A) indicated that some areas do not contain iron while others are very rich. The Mg/Si atomic ratio was generally close to 2 as in the Olivine structure of (Mg<sub>2</sub>SiO<sub>4</sub>). In iron-rich areas, the Mg/Si ratio increased markedly, indicating that Fe is generally associated with Mg.

**Fresh Fe/olivine:** The SEM analysis of the fresh Fe/Olivine samples showed almost complete coverage of Olivine grains by added iron oxide. In fact, the angular morphology of the support was not visible any more on this sample (Fig. 5). The EDX analysis indicated that the iron oxide was not distributed evenly throughout the Olivine grain. Higher concentrations than those observed for the Olivine sample were observed on the Fe/Olivine sample (Fig. A.6, Appendix A).

**Fe/Oliv-1 h and Fe/Oliv-2 h:** The SEM analysis of the Fe/Oliv-1 h sample showed that Olivine grains were still covered by iron oxide after 1 h of TOS (Fig. 6 left). However, the iron particles appeared to be more agglomerated than on the raw Fe/Olivine sample. The EDX analysis (Fig. A.7, Appendix A) showed a more irregular distribution of iron oxide over the entire Olivine grain compared to the raw Fe/Olivine sample, the analysed areas being even richer in iron. These zones were again associated with the highest Mg/Si ratios. Similar observations can be reported for the Fe/Oliv-2 h sample for both, morphology (Fig. 6 right) and EDX analysis (Fig. A.8, Appendix A). The values of the Mg/Si ratio were very variable in this sample and elemental carbon was sometimes observed.

**Fe/Oliv-4 h:** SEM analysis of the Fe/Oliv-4 h samples indicated a very discontinuous coverage of the Olivine grains by iron oxide after 4 h of TOS (Fig. 7). Indeed, the analysis revealed the formation of iron oxide agglomerates (white because analysed by back-scattered electron detector) on the surface of the olivine grains as iron oxides crystals or very well crystallized agglomerates (rather spherical) aligned on parallel axes. In this case, iron oxide was distributed over the entire Olivine grain in a very variable manner; the analysed areas were very rich in iron (Fig. A.9, Appendix A) and the Mg/Si ratio was very variable. Elemental carbon (up to 5.8 atomic% or 2.5 wt%), as well as elements from biomass (Al, Ca) were occasionally observed.

**Fe/Oliv HGF-2:** The SEM analysis of the Fe/oliv HGF-2 sample (Fig. 8) revealed that after 8 h of TOS (2 successive tests of 4 h), the surface of the Olivine grains was covered with agglomerates of very variable size (200 nm < dp < 6 µm). The EDX analysis indicated some iron rich areas (Fig. A.10, appendix A), confirming that the iron oxide was distributed over the Olivine grain in an even more variable manner. Elemental carbon, as well as elements from biomass (Al, Ca) were

reported and occasionally, in very high concentrations.

Results of the TPO analysis were depicted in Fig. 9. Overall, the comparison of the TPO curves showed that the amount of carbon increases with the TOS. Moreover, the TPO profile of the sample Fe/Oliv-1 h (shorter TOS) indicated that the oxidation begins at low temperature (around 350 °C) and takes place in two separated peaks with maximum around 500 and 600 °C, respectively. This behaviour was associated with two carbon forms on the sample (iron carbide and carbon filaments, respectively [35]), the stability depending on their structure. For the rest of iron-doped samples, the stability of the carbon formed appeared to increase with the increasing value of TOS. Indeed, the first of the two peaks originally observed for the sample Fe/Oliv-1 h (low TOS), was progressively shifted to higher temperature until it disappeared for the sample Fe/Oliv HGF-2 (high TOS). In the latter case, the TPO profile showed a maximum between 570 and 590 °C. For all samples, the carbon oxidation ended approximatively at the same temperature (650 °C). In the case of the used non-doped olivine sample (REF), the oxidation started around 480 °C and showed a single maximum peak at 600 °C.

Moreover, the amount of carbon deposited on each sample was reported in Fig. 10 in terms of percentage of the masse sample. The higher the TOS, the more elevated carbon amount is deposited on the sample. Furthermore, the carbon formation rate (in gram of carbon per gram of the catalyst and per hour of TOS) indicated a maximum for the lowest TOS studied with Fe/Olivine catalyst. The values decreased linearly when TOS increased. In fact, it is well known that carbon formation rate is no constant due to an equilibrium between hydrocarbons decomposition (from biomass) and carbon gasification (by oxygen, steam, and carbon dioxide). These values were in the range previously described for this type of catalyst [30]. In line with [21], the lower carbon formation rate observed for REF (non-doped Olivine) compared to Fe/Olivine samples can be explained by the lower activity of the support.

### 3.3. In-bed elimination of tars: Combined effect of char and Fe/Olivine

Table 2 summarizes the results of gasification output indicators and product yields for all tests. In addition, the individual yields of all quantified molecules were reported in Table B.1, Appendix B. Compared to REF, the values of the LHV, CGE and carbon yield obtained for the test Fe/Oliv-2 h dropped by ca. 10 %, probably linked to the decrease in the concentration of CH<sub>4</sub> and C<sub>2</sub>-C<sub>3</sub> hydrocarbons, as well as, to the effect of char accumulation. The latter drop is reduced to only 5 % if the mass of the char accumulated inside the reactor is subtracted from the mass of feed. Table B.2.

Within the tests of the second series (Fe/Oliv-1 h, Fe/Oliv-2 h, Fe/Oliv-4 h), slight differences were observed in the gas yields with increasing TOS but the simultaneous variation of other parameters, such as: mass of olivine inside the reactor, char hold-up and gas residence time, makes difficult the identification of the precise reactional mechanisms at the origin of these trends. Indeed, the variations in gas composition were probably linked to the simultaneous effect of several reactions in homogeneous and heterogeneous phases, such as char gasification by CO<sub>2</sub> (C + CO<sub>2</sub> → 2CO) and H<sub>2</sub>O (C + H<sub>2</sub>O → CO + H<sub>2</sub>), as well as light hydrocarbons steam reforming.

Regarding the tar content, the results of quantitative analysis showed a drop of ca. 50 % in the overall tar yield for the tests of the second series with respect to REF (see Table 2). The reduction in the content of light and heavy PAH was confirmed by the drop in the overall intensity of Synchronous Fluorescence Spectra as shown in Fig. 11. However, tar content was relatively unchanged within the series. A possible explanation for the unchanged tar content with TOS is the occurrence of two simultaneous phenomena with a opposite effect on tar abatement: On

the one hand, the loss of the catalytic activity of the Fe/olivine particles because of surface attrition and, on the other hand, the gain in tar abatement activity with increasing char hold-up inside the reactor. Finally, the yield of  $\text{NH}_3$  and HCN was only determined for the test Fe/Oliv-2 h. The results indicated a slight reduction in the yield of both molecules compared to REF.

### 3.4. Effect of In-bed elimination of tars coupled with oxidative Hot gas filtration

The values of the gasification output indicators and products yields for the two consecutive HGF tests of the third series were included in Table 2. In general, and compared to REF, the integration of the oxidative HGF unit led to a rise and a drop in the gas yield and LHV, respectively. In the case of the second test (Fe/Oliv HGF-2), the values of CGE, %C and %H rose notably indicating the partial oxidation of carbon rich particles accumulated on the surface of the filter. Similarly to previous study [15], the 80–90 °C gap measured between the dirty and the clean side of the filter support this mechanism.

Regarding the tar content, the results indicated a 70 % drop in the overall tar yield for both HGF tests compared to REF. The results of quantitative analysis were corroborated by the substantial drop in the intensity of Synchronous Fluorescence Spectra as shown in the Fig. 11. In terms of composition, all tars groups (II, III, IV and V) showed a decrease of more than 50 %. Temperatures inside the HGF unit were relatively low to promote catalytic cracking reactions of tars [15]. Therefore, condensation and polymerisation of tar molecules were likely the main mechanisms behind the drop observed in the tar yield. Moreover, the reduction in the content of light and heavy PAH (tars of class IV and V), resulted in a considerable diminution of the tar dew point of the producer gas leading to temperatures of about 80 °C for the two filtration tests (see Table 2). These low tar dew point values were below the maximum intake temperature for a spark ignition engine to ensure knock-free operation (about 100 °C) [48], but still higher than the intake temperature for a standard engine, typically about 40 °C [49]. The utilisation of an homogeneous charge compression ignition engine allowing intake temperatures as high as 250 °C [2] could be an alternative to avoid an intermediary tar clean-up stage downstream de HGF unit.

On the other hand, the visual inspection of the filter unit after the test Fe/Oliv HGF-2 revealed the formation of a filter cake of approx. 5–10 mm thickness, loosely adhered that felt spontaneously during offline cleaning operations. To get a further insight on the state of the filter surface, a sample of 1–2  $\text{cm}^2$  of the filter mesh was carefully extracted from the middle part of the filtration cartridge and then, analysed by SEM-EDX. The SEM images of the dirty side, depicted in Fig. 12, revealed an outer surface fairly clear with disperse deposits composed mostly of particles with a particle size ranging from 1 to 10  $\mu\text{m}$ . Particle deposits appeared to be loosely adhered to the surface of the metallic wires. Moreover, EDX spot analyses conducted on several points of the filter surface (see Table B.3, appendix B), confirmed that these deposits were mainly composed of Fe-rich particles elutriated from the reactor.

## 4. Conclusions

Gasification experiments were carried out in a pilot scale fluidized bed reactor operated under allothermal mode at constant temperature and low fluidisation regime ( $U_0/U_{mf} \approx 2-3$ ) with a twofold objective: (i) assess the combined effect of iron-doped olivine, char hold-up and oxidative hot gas filtration on tar abatement and, (ii) determine the effect of TOS on the properties of iron-doped olivine.

The determination of the weight and particle size distribution of the components of the bed inventory after each test revealed that catalyst elutriation and char hold-up took place to a large extent. Interparticle mechanical attrition, mostly surface abrasion, was the main mechanism dominating the reduction of the particle size. On the other hand, char

hold-up was linked to the low char conversion inside the reactor probably originated from the poor lateral and axial mixing, lower attrition, and elutriation of char particles.

The characterization of fresh and used catalyst revealed:

- Loss in iron oxides during the first hour of test due to attrition and partial reduction of hematite to magnetite and wustite but stable composition for higher TOS.
- Amount of reducible iron oxides present in the surface of the Fe/olivine decreased initially but then stabilised (TOS greater than 4 h) at a value twice as high as the fresh non-doped olivine.
- SEM observation confirmed the loss of the iron oxide coverage of Fe/olivine particles with increasing TOS and the formation of agglomerates mainly composed of iron oxides crystals.
- The amount of carbon deposited in the surface of the Fe/olivine particles increased with TOS, but in any case, these carbon deposits were completely oxidized at temperatures above 650 °C.

The in-bed tar abatement strategy combining the Fe/olivine catalyst and char hold-up tested in this study resulted in a reduction of 50 % in the overall tar yield with respect to the reference values. Nevertheless, the simultaneous variation of several reactor parameters (mass of catalyst inside the reactor, char hold-up and gas residence time) with TOS made difficult the precise identification of the reactional mechanisms at the origin of the drop in the tar yield.

Furthermore, the combination of the in-bed materials (Fe/Olivine + char) and the oxidative HGF unit, lead to a drop in overall tar yield of 70 % with respect to the reference tests. The tar dew point of the resulting producer gas was estimated to 80 °C. Latter value is only 40 °C above the threshold value recommended for its valorisation in standard internal combustion engines. Finally, the SEM-EDX observation of the surface of the HGF cartridges revealed loosely adhered deposits mainly composed of very fine iron-rich particles.

To conclude, the explored combination of primary and secondary methods to reduce tar concentration in syngas is performant, but it should be assessed for longer operation time (days and even weeks). These type of tests would allow to determine if it is necessary to improve the resistance of Fe doped olivine to attrition.

### CRedit authorship contribution statement

**Miguel Ruiz:** Conceptualization, Methodology, Investigation, Visualization, Formal analysis, Writing – original draft, Writing – review & editing, Project administration. **Adam Schitzer:** Investigation. **Claire Courson:** Formal analysis, Validation, Writing – review & editing, Funding acquisition. **Guillain Mauviel:** Writing – review & editing, Project administration, Supervision, Funding acquisition.

### Declaration of Competing Interest

The authors declare that they have no known competing financial interests or personal relationships that could have appeared to influence the work reported in this paper.

### Acknowledgements

The authors thank the ADEME, France (Adelither – project N°1702C0042) and the Region Grand-Est, France (Feder Project Hy-C-Green) for the financial support.

### Appendix A

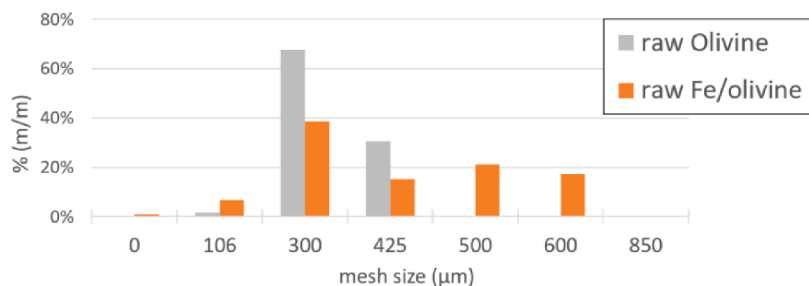


**Fig. A1.** Particle size distribution of the raw olivine catalyst before and after iron addition. Particle size distribution was determined by sieving. Analyses were conducted after slight agitation for 10 min

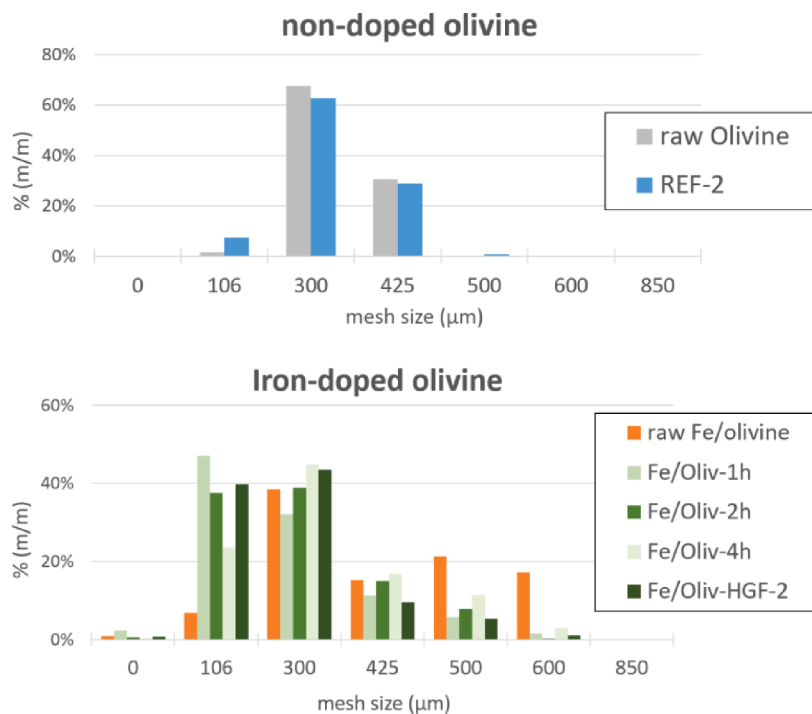


**Fig. A2.** Particle size distribution of raw and used olivine catalysts. Particle size distribution was determined by sieving. Analyses were conducted after slight agitation for 10 min.

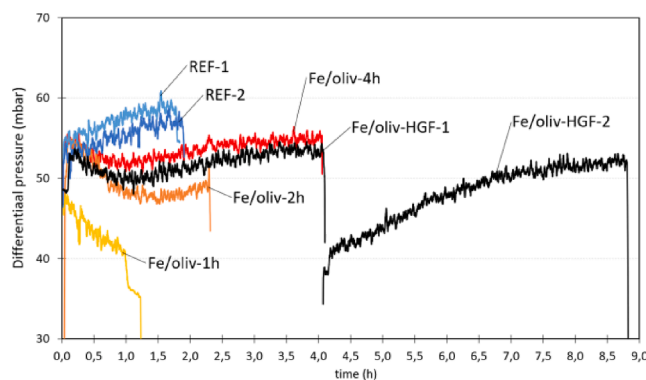


**Fig. A3.** Pressure drop profiles across the fluidized bed reactor. Pressure drop was determined as the difference between the pressure under the grid and the pressure at the top of the reactor. The relatively low value of the initial pressure drop of the test Fe/Oliv-1h was due to a back-up pressure caused by a plug formed downstream the heat exchangers. The gap in the initial pressure drop between the tests Fe/Oliv HGF-1 and Fe/Oliv HGF-2 was due to the difference in the mass of Fe/Olivine loaded in the reactor at the beginning of each test, equals to 4 kg and 3 kg, respectively.

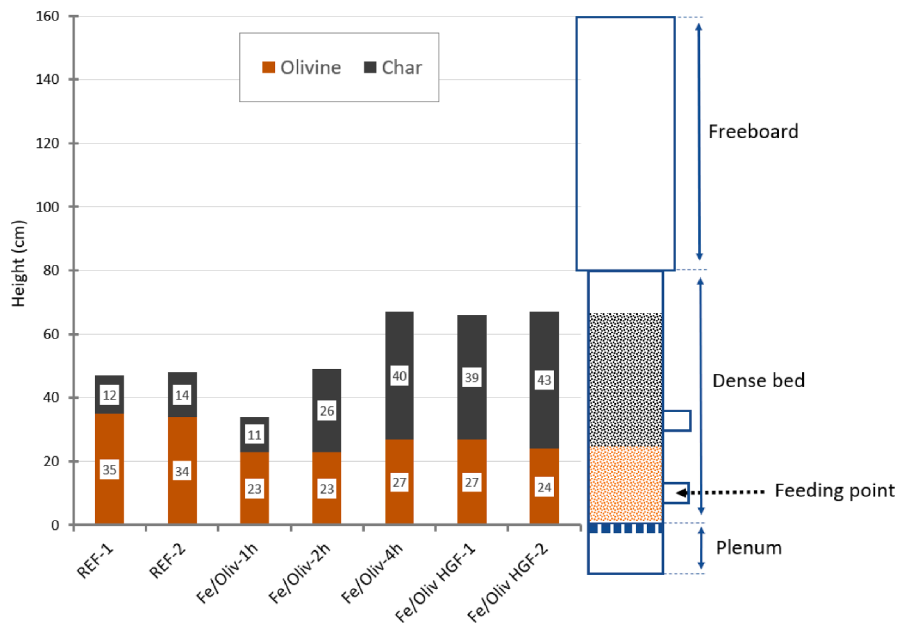


Fig. A4. Comparison of the estimated height of the bed material inventories with the dimensions of the gasification reactor. To carry out these measures, the bed material inventories recovered after each test were poured in a transparent cylinder at ambient temperature.

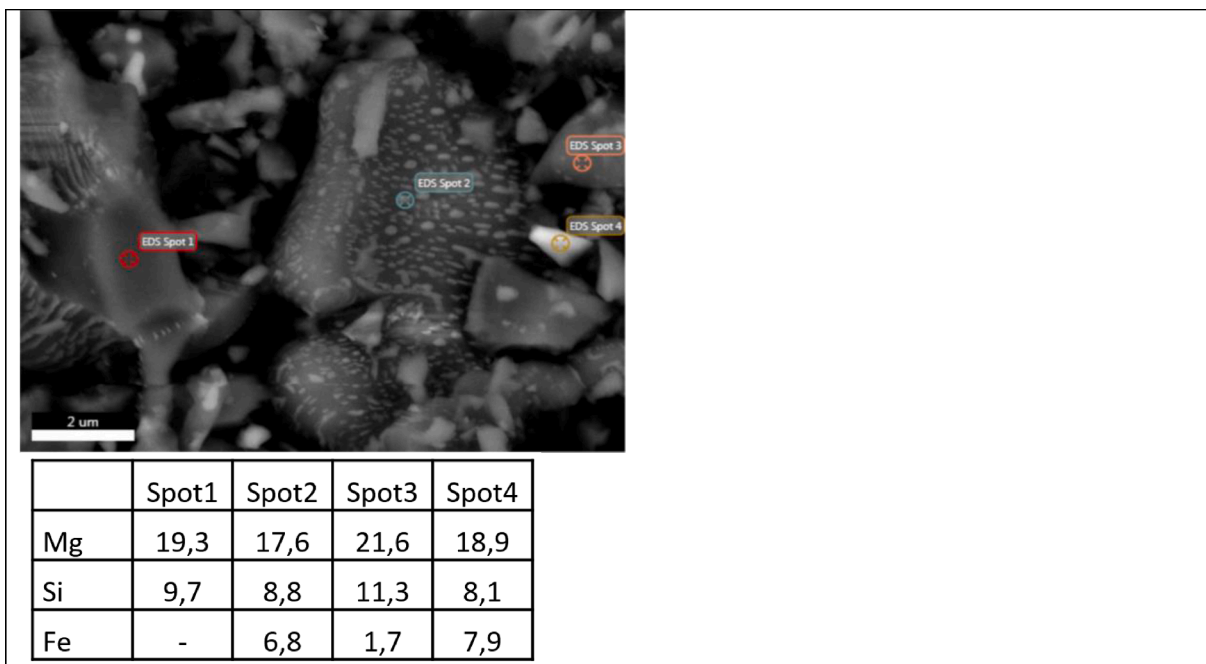


Fig. A5. SEM-EDX analysis of a sample of fresh non-doped olivine.

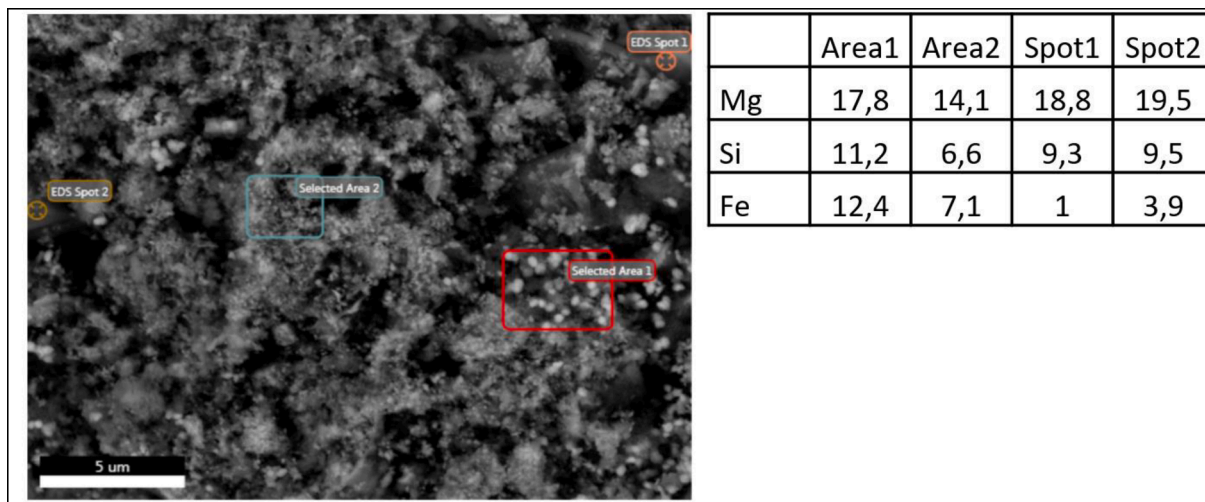


Fig. A6. SEM-EDX analysis of a sample of fresh raw Fe/olivine.

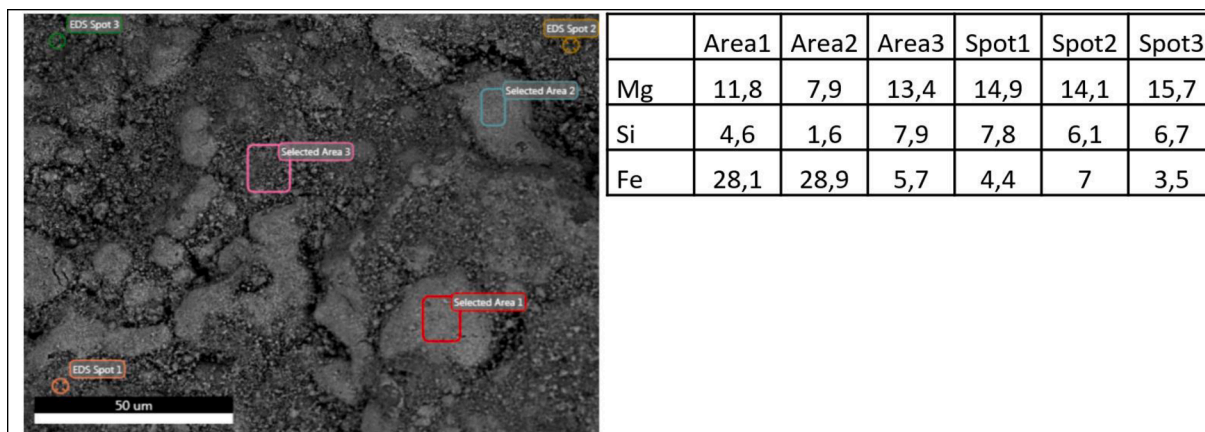


Fig. A7. SEM-EDX analysis of a sample of Fe/oliv-1h.

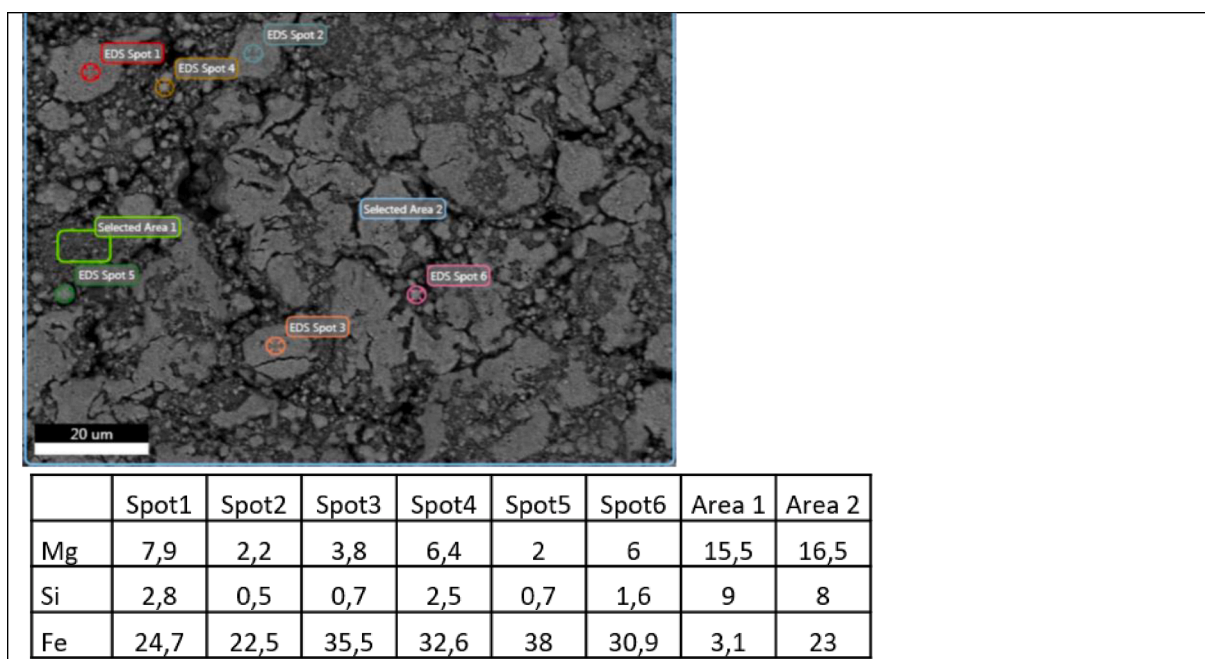


Fig. A8. SEM-EDX analysis of a sample of Fe/oliv-2h.



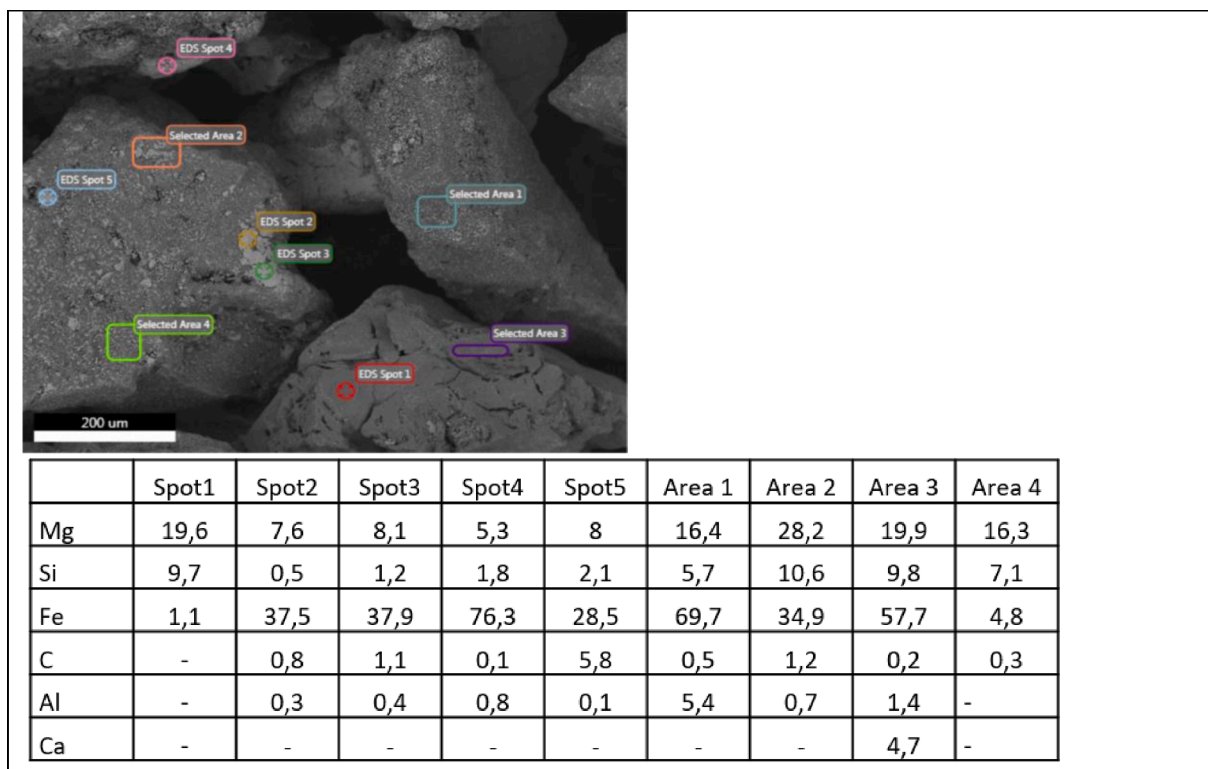


Fig. A9. SEM-EDX analysis of a sample of Fe/oliv-4h.

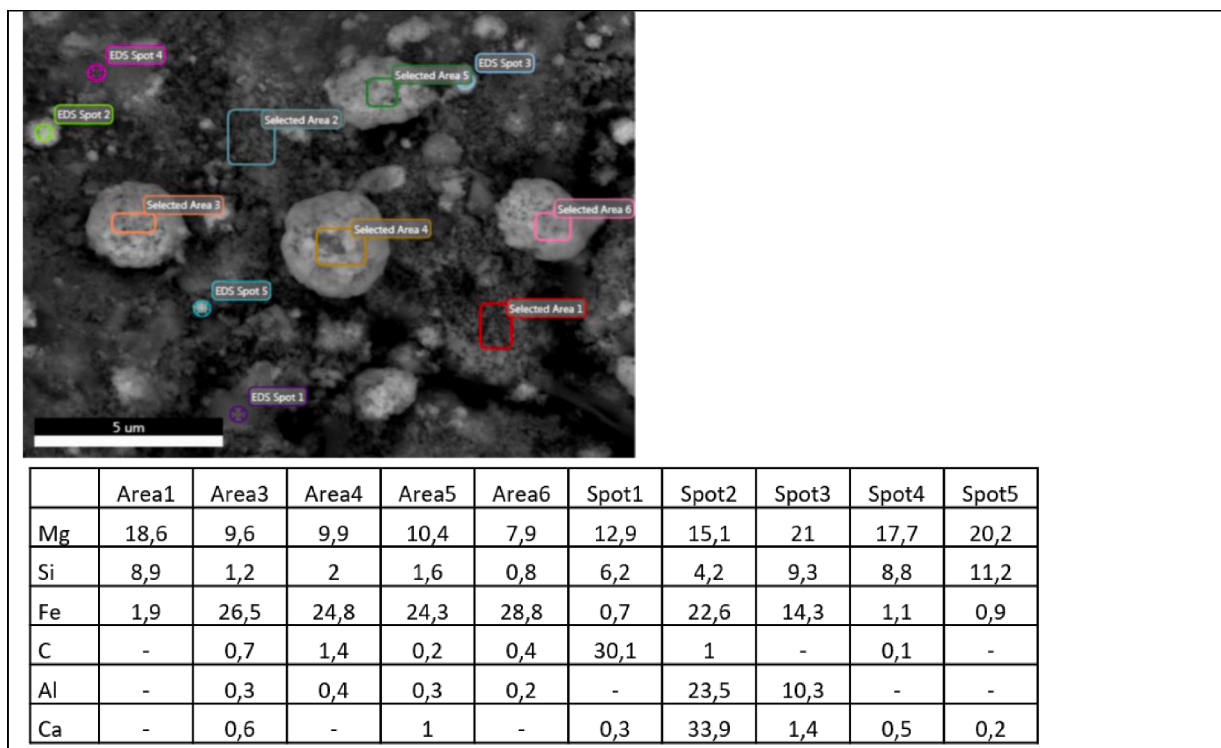


Fig. A10. SEM-EDX analysis of a sample of Fe/oliv-HGF-2

## Appendix B

Table B4

Table B1

Yields results of all quantified molecules (expressed in g/kg feed (daf)). To express the results in concentration units, individual values must be divided by the gas yield detailed in.

Tar Class	REF	Fe/oliv 1 h	Fe/oliv 2 h	Fe/oliv 4 h	Fe/oliv + HGF-1	Fe/oliv + HGF-2	
–	H2	12 ± 1	13	13	16	16	18
–	CO	235 ± 17	178	195	241	237	275
–	CO2	508 ± 8	520	507	456	566	618
–	CH4	43 ± 1	38	36	38	39	46
–	C2H4	22.2 ± 0.4	15.9	16.6	14.9	15.3	17.5
–	C2H6	3.2 ± 0.2	1.9	2.1	2.0	2.0	2.3
–	C2H2	1.8 ± 0.2	0.8	0.8	0.6	0.3	0.6
–	C3H6	2.2 ± 0.7	0.8	1.8	1.5	1.2	1.3
–	C3H4	0.17 ± 0.04	0.08	0.17	0.20	0.16	0.11
–	N2	1732 ± 4	1706	1756	1440	1649	1630
–	O2	11 ± 2	21	25	58	37	1
–	benzene	6.45 ± 0.08	6.15	4.62	4.59	4.98	5.07
III	toluene	2.12 ± 0.03	1.40	1.21	1.34	1.04	1.03
III	o-xylene	0 ± 0	0	0	0	0	0
III	p-xylene	0.24 ± 0.01	0.14	0.12	0.14	0.08	0.10
III	phenylethyne	0.09 ± 0.01	0	0	0	0	0
III	styrene	0.88 ± 0.01	0.45	0.40	0.41	0.23	0.25
II	phenol	0.24 ± 0.02	0	0	0	0	0
II	benzofuran	0.20 ± 0.01	0	0.07	0.08	0.05	0.06
III	indene	0.92 ± 0.01	0.32	0.30	0.33	0.04	0.05
II	4-methyl-phenol	0 ± 0	0	0	0	0	0
III	2-methyl-indene	0.038 ± 0.002	0	0	0	0	0
III	3-methyl-1H-indene	0.06 ± 0.01	0	0	0	0	0
III	1-ethylidene-1H-Indene	0.215 ± 0.001	0.030	0.100	0.107	0.039	0.044
IV	2-methyl-naphthalene	0.18 ± 0.01	0.10	0.09	0.10	0.04	0.04
IV	biphenyl	0.069 ± 0.003	0	0	0	0	0
IV	2-ethenyl-naphthalene	0.065 ± 0.002	0	0	0	0	0
IV	Naphthalene	1.49 ± 0.08	1.01	0.77	0.80	0.55	0.58
IV	Acenaphthylene	0.93 ± 0.06	0.43	0.44	0.52	0.10	0.13
IV	Acenaphtene	0 ± 0	0	0	0	0	0
IV	Fluorene	0.39 ± 0.01	0.16	0.15	0.12	0.02	0.02
IV	Phenanthrene	0.20 ± 0.01	0.15	0.12	0.09	0.04	0.05
IV	Anthracene	0.087 ± 0.003	0.043	0.036	0.027	0.006	0.008
IV	Fluoranthene	0.13 ± 0.02	0.06	0.06	0.03	0.01	0.02
V	Pyrene	0.13 ± 0.01	0.07	0.06	0.07	0.03	0.03
V	Benzo[a]anthracene	0.019 ± 0.004	0.008	0.006	0	0	0
V	Chrysene	0.019 ± 0.006	0.009	0.007	0.003	0	0
V	Benzo[b]fluoranthene	0.0058 ± 0.0008	0.004	0.003	0	0	0
V	Benzo[k]fluoranthene	0.0025 ± 0.0003	0	0	0	0	0
V	Benzo[a]pyrene	0.012 ± 0.001	0.0031	0.0025	0	0	0
V	Dibenzo[a,h]anthracene	0 ± 0	0	0	0	0	0
V	Benzo[ghi]perylene	0 ± 0	0	0	0	0	0
V	Indeno[1,2,3-cd]pyrene	0.0033 ± 0.0021	0	0	0	0	0

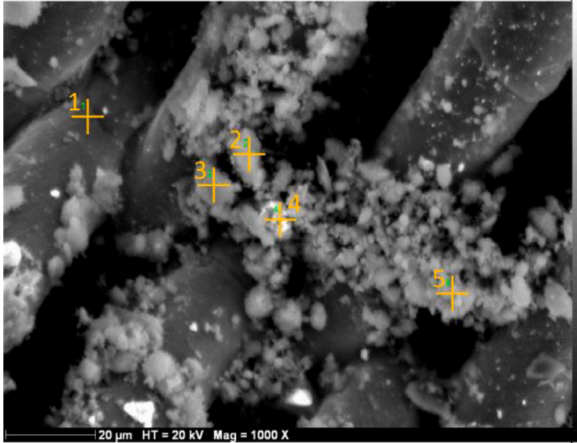
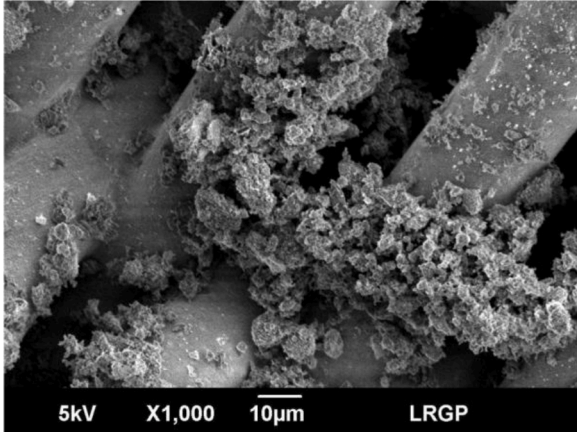
Table B2

Gasification yield calculated including the total flow of N<sub>2</sub> injected into the system.

	REF	Fe/oliv 1 h	Fe/oliv 2 h	Fe/oliv 4 h	Fe/oliv + HGF-1	Fe/oliv + HGF-2
Gas Yield, Nm <sup>3</sup> /kg <sub>feed</sub> (daf)	2.05 ± 0.03	2.01	2.03	1.84	2.06	2.10

**Table B3**

SEM-EDX spot analysis of the dirty side of the filter cartridge after the test Fe/oliv-HGF-2. Image (A) and (B) were taken with an accelerating voltage of 20 kV and 5 kV, respectively, for a better visualisation of the morphology of the deposit. Yellow crosses show the points (spots) where the EDX analysis was carried out. Elemental composition is expressed in mass basis.

Image A	Element	wt.% (by EDX)				
		spot1	spot2	spot3	spot4	spot5
	C	6,7	3,77	3,79	2,25	4,51
	O	10,98	43,45	39,75	42,69	39,76
	Na	0,34	0,43	0,11	0	0,26
	Mg	1,35	19,4	17,07	25,19	18,46
	Al	0,22	0,17	0,08	0,08	0,12
	Si	1,08	11,49	20,28	19,32	11,02
	P	0,23	0,12	0,09	0,09	0,09
	S	1,03	0,1	0,14	0,08	0,17
	K	0,06	0,07	0,09	0,1	0,12
	Ca	0,08	0,07	0,1	0,1	0,21
	Cr	14,81	0,57	1,21	0,31	1,72
	Mn	0,37	0,05	0,06	0,19	0
	Fe	54,64	19,76	16,36	8,05	22,64
	Ni	7,66	0,24	0,42	0,66	0,52
	Zn	0,44	0,29	0,45	0,88	0,4
Image B						
						

**Table B4**

Feedstock analysis. Proximate analysis was conducted according to French standards NF EN ISO18134. Ultimate analysis was conducted according to standards ISO 16,948 and ISO 16994. MDF typically presents a high content in Fuel Bounded Nitrogen (FBN) due to the utilisation of urea–formaldehyde resin for its production. Ash melting temperatures of biomass samples were determined according to French standard CEN/TS 15370–1.

Composition of MDF feedstock	
Moisture, wt. %	8.6
Volatile content, wt. % (db)	88
Ash wt. % (dry base)	0.42
<b>Ultimate analysis, wt. % (db)</b>	
C	49.6
H	6.02
N	3.47
S	0.008
Cl	0.005
O <sub>calculated by difference</sub>	40.48
<b>Major metallic elements in Ash composition, mg/kg<sub>feedstock</sub> (db)</b>	
Ca	791
K	890
Mn	111
Mg	274
Na	61
P	91
Si	<100
<b>Minor metallic elements in Ash composition, mg/kg<sub>feedstock</sub> (db)</b>	
As	<0.8
Al	45
Cd	<0.2
Cr	<1
Cu	1
Fe	41
Ni	<1
Pb	<2
Zn	16
Hg	<0.05
Co	<1
Mo	<2
Ti	3
Sb	<1
V	<1
<b>Ash melting temperatures (°C)</b>	
Initial deformation temperature	1070
Softening temperature	1420
Hemispherical temperature	1460
Fluid temperature	1490

## References

- [1] M.L. Valderrama Rios, A.M. González, E.E.S. Lora, O.A. Almazán del Olmo, Reduction of tar generated during biomass gasification: A review, *Biomass Bioenergy* 108 (2018) 345–370, <https://doi.org/10.1016/j.biombioe.2017.12.002>.
- [2] S. Bhaduri, B. Berger, M. Pochet, H. Jeanmart, F. Contino, HCCI engine operated with unscrubbed biomass syngas, *Fuel Process. Technol.* 157 (2017) 52–58, <https://doi.org/10.1016/j.fuproc.2016.10.011>.
- [3] L. Devi, K.J. Ptasiński, F.J.J.G. Janssen, A review of the primary measures for tar elimination in biomass gasification processes, *Biomass Bioenergy* 24 (2003) 125–140, [https://doi.org/10.1016/S0961-9534\(02\)00102-2](https://doi.org/10.1016/S0961-9534(02)00102-2).
- [4] P.J. Woolcock, R.C. Brown, A review of cleaning technologies for biomass-derived syngas, *Biomass Bioenergy* 52 (2013) 54–84, <https://doi.org/10.1016/j.biombioe.2013.02.036>.
- [5] E. Kurkela, M. Kurkela, I. Hiltunen, Steam–oxygen gasification of forest residues and bark followed by hot gas filtration and catalytic reforming of tars: Results of an extended time test, *Fuel Process. Technol.* 141 (2016) 148–158, <https://doi.org/10.1016/j.fuproc.2015.06.005>.
- [6] J. Corella, J.M. Toledo, R. Padilla, Olivine or Dolomite as In-Bed Additive in Biomass Gasification with Air in a Fluidized Bed: Which Is Better? *Energy Fuels* 18 (2004) 713–720, <https://doi.org/10.1021/ef0340918>.
- [7] L. Devi, K.J. Ptasiński, F.J.J.G. Janssen, S.V.B. van Paasen, P.C.A. Bergman, J.H. A. Kiel, Catalytic decomposition of biomass tars: use of dolomite and untreated olivine, *Renewable Energy* 30 (2005) 565–587, <https://doi.org/10.1016/j.renene.2004.07.014>.
- [8] G. Ravenni, Z. Sárossy, J. Ahrenfeldt, U.B. Henriksen, Activity of chars and activated carbons for removal and decomposition of tar model compounds – A review, *Renew. Sustain. Energy Rev.* 94 (2018) 1044–1056, <https://doi.org/10.1016/j.rser.2018.07.001>.
- [9] X. Zeng, Y. Ueki, R. Yoshiie, I. Naruse, F. Wang, Z. Han, et al., Recent progress in tar removal by char and the applications: A comprehensive analysis, *Carbon Resources Conversion* 3 (2020) 1–18, <https://doi.org/10.1016/j.crcon.2019.12.001>.
- [10] NOTAR® Gasifier. Xylowatt n.d. <https://www.xylowatt.com/notar-gasifier/> (accessed March 3, 2021).
- [11] P. Brandt, E. Larsen, U. Henriksen, High Tar Reduction in a Two-Stage Gasifier, *Energy Fuels* 14 (2000) 816–819, <https://doi.org/10.1021/ef990182m>.
- [12] X. Zeng, F. Wang, Z. Han, Y. Sun, Y. Cui, G. Xu, Characterization and pilot scale test of a fluidized bed two-stage gasification process for the production of clean industrial fuel gas from low-rank coal, *Carbon Resources Conversion* 1 (2018) 73–80, <https://doi.org/10.1016/j.crcon.2018.05.003>.
- [13] S. Tuomi, E. Kurkela, P. Simell, M. Reinikainen, Behaviour of tars on the filter in high temperature filtration of biomass-based gasification gas, *Fuel* 139 (2015) 220–231, <https://doi.org/10.1016/j.fuel.2014.08.051>.
- [14] L. Lang, W. Yang, J. Xie, X. Yin, C. Wu, J.Y.S. Lin, Oxidative filtration for flyash & tar removal from 1.0 MWth fixed-bed biomass air gasification, *Biomass Bioenergy* 122 (2019) 145–155, <https://doi.org/10.1016/j.biombioe.2019.01.018>.
- [15] M. Ruiz, A. Schnitzer, P. Arnoux, G. Mauviel, Gasification of N-rich fibreboard in an air-blown fluidized bed reactor: A study on the fate of tars, NH<sub>3</sub> and HCN during oxidative mild Hot Gas Filtration, *Fuel* 303 (2021), 121317, <https://doi.org/10.1016/j.fuel.2021.121317>.
- [16] S. Rapagnà, N. Jand, A. Kiennemann, P.U. Foscolo, Steam-gasification of biomass in a fluidised-bed of olivine particles, *Biomass Bioenergy* 19 (2000) 187–197, [https://doi.org/10.1016/S0961-9534\(00\)00031-3](https://doi.org/10.1016/S0961-9534(00)00031-3).
- [17] C. Chr, D. Grimekis, K.D. Panopoulos, E.P. Pachatouridou, E.F. Iliopoulou, E. Kakaras, Comparing calcined and un-treated olivine as bed materials for tar reduction in fluidized bed gasification, *Fuel Processing Technology* 124 (2014) 275–285, <https://doi.org/10.1016/j.fuproc.2014.03.012>.
- [18] R. Michel, M.R. Ammar, E. Véron, P. Simon, J. Poirier, Investigating the mechanism of phase transformations and migration in olivine at high temperature, *RSC Adv.* 4 (2014) 26645–26652, <https://doi.org/10.1039/C4RA01238K>.

- [19] M. Kądziołka-Gaweł, Z. Adamczyk, L. Kalinowski, M. Össbauer, Study of Changes in Olivine After Heating in Air, *Canad. Mineral.* 57 (2019) 105–115, <https://doi.org/10.3749/canmin.1700074>.
- [20] M. Virginie, C. Courson, D. Niznansky, N. Chaoui, A. Kiennemann, Characterization and reactivity in toluene reforming of a Fe/olivine catalyst designed for gas cleanup in biomass gasification, *Appl. Catal. B* 101 (2010) 90–100, <https://doi.org/10.1016/j.apcatb.2010.09.011>.
- [21] D. Świerczyński, C. Courson, L. Bedel, A. Kiennemann, S. Vilminot, Oxidation Reduction Behavior of Iron-Bearing Olivines (FexMg1-x)2SiO4 Used as Catalysts for Biomass Gasification, *Chem. Mater.* 18 (2006) 897–905, <https://doi.org/10.1021/cm051433+>.
- [22] J. Meng, X. Wang, Z. Zhao, A. Zheng, Z. Huang, G. Wei, et al., Highly abrasion resistant thermally fused olivine as in-situ catalysts for tar reduction in a circulating fluidized bed biomass gasifier, *Bioresour. Technol.* 268 (2018) 212–220, <https://doi.org/10.1016/j.biortech.2018.07.135>.
- [23] C. Courson, E. Makaga, C. Petit, A. Kiennemann, Development of Ni catalysts for gas production from biomass gasification. Reactivity in steam- and dry-reforming, *Catal. Today* 63 (2000) 427–437, [https://doi.org/10.1016/S0920-5861\(00\)00488-0](https://doi.org/10.1016/S0920-5861(00)00488-0).
- [24] J.N. Kuhn, Z. Zhao, A. Senefeld-Naber, L.G. Felix, R.B. Slimane, C.W. Choi, et al., Ni-olivine catalysts prepared by thermal impregnation: Structure, steam reforming activity, and stability, *Appl. Catal. A* 341 (2008) 43–49, <https://doi.org/10.1016/j.apcata.2007.12.037>.
- [25] Y. Tursun, S. Xu, A. Abulikemu, T. Dilinuer, Biomass gasification for hydrogen rich gas in a decoupled triple bed gasifier with olivine and NiO/olivine, *Bioresour. Technol.* 272 (2019) 241–248, <https://doi.org/10.1016/j.biortech.2018.10.008>.
- [26] T. Nordgreen, V. Nemanova, K. Engvall, K. Sjöström, Iron-based materials as tar depletion catalysts in biomass gasification: Dependency on oxygen potential, *Fuel* 95 (2012) 71–78, <https://doi.org/10.1016/j.fuel.2011.06.002>.
- [27] P.A. Simell, J.K. Leppälähti, J.B. Bredenberg, Catalytic purification of tarry fuel gas with carbonate rocks and ferrous materials, *Fuel* 71 (1992) 211–218, [https://doi.org/10.1016/0016-2361\(92\)90011-C](https://doi.org/10.1016/0016-2361(92)90011-C).
- [28] T. Nordgreen, T. Liliedahl, K. Sjöström, Elemental Iron as a Tar Breakdown Catalyst in Conjunction with Atmospheric Fluidized Bed Gasification of Biomass: A Thermodynamic Study, *Energy Fuels* 20 (2006) 890–895, <https://doi.org/10.1021/ef0502195>.
- [29] V. Nemanova, T. Nordgreen, K. Engvall, K. Sjöström, Biomass gasification in an atmospheric fluidised bed: Tar reduction with experimental iron-based granules from Höganäs AB, Sweden, *Catalysis Today* 176 (2011) 253–257, <https://doi.org/10.1016/j.cattod.2010.12.019>.
- [30] S. Rapagnà, M. Virginie, K. Gallucci, C. Courson, M. Di Marcello, A. Kiennemann, et al., Fe/olivine catalyst for biomass steam gasification: Preparation, characterization and testing at real process conditions, *Catal. Today* 176 (2011) 163–168, <https://doi.org/10.1016/j.cattod.2010.11.098>.
- [31] Z. Yu, Y. Yang, S. Yang, Q. Zhang, J. Zhao, Y. Fang, et al., Iron-based oxygen carriers in chemical looping conversions: A review, *Carbon Resources Conversion* 2 (2019) 23–34, <https://doi.org/10.1016/j.crcon.2018.11.004>.
- [32] J. Meng, Z. Zhao, X. Wang, J. Chen, A. Zheng, Z. Huang, et al., Steam reforming and carbon deposition evaluation of phenol and naphthalene used as tar model compounds over Ni and Fe olivine-supported catalysts, *J. Energy Inst.* 92 (2019) 1765–1778, <https://doi.org/10.1016/j.joei.2018.12.004>.
- [33] V. Claude, J.G. Mahy, S. Douven, S.L. Pirard, C. Courson, S.D. Lambert, Ni- and Fe-doped  $\gamma$ -Al<sub>2</sub>O<sub>3</sub> or olivine as primary catalyst for toluene reforming, *Mater. Today Chem.* 14 (2019), 100197, <https://doi.org/10.1016/j.mtchem.2019.100197>.
- [34] Fredriksson HOA, Lancee R.J., Thüne P.C., Veringa H.J., Niemantsverdriet J.W. (Hans). Olivine as tar removal catalyst in biomass gasification: Catalyst dynamics under model conditions. *Appl. Catal. B: Environ.* 2013, 130–131:168–77. 10.1016/j.apcatb.2012.10.017.
- [35] M. Virginie, J. Adánez, C. Courson, L.F. de Diego, F. García-Labiano, D. Niznansky, et al., Effect of Fe–olivine on the tar content during biomass gasification in a dual fluidized bed, *Appl. Catal. B* 121–122 (2012) 214–222, <https://doi.org/10.1016/j.apcatb.2012.04.005>.
- [36] Y. Pan, A. Abulizi, D. Talifu, Y. Tursun, S. Xu, Catalytic gasification of biomass and coal blend with Fe<sub>2</sub>O<sub>3</sub>/olivine in a decoupled triple bed, *Fuel Process. Technol.* 194 (2019), 106121, <https://doi.org/10.1016/j.fuproc.2019.106121>.
- [37] T.A. Brown, F. Scala, S.A. Scott, J.S. Dennis, P. Salatino, The attrition behaviour of oxygen-carriers under inert and reacting conditions, *Chem. Eng. Sci.* 71 (2012) 449–467, <https://doi.org/10.1016/j.ces.2011.11.008>.
- [38] Y. Tsuboi, S. Ito, M. Takafuji, H. Ohara, T. Fujimori, Development of a regenerative reformer for tar-free syngas production in a steam gasification process, *Appl. Energy* 185 (2017) 1217–1224, <https://doi.org/10.1016/j.apenergy.2015.12.110>.
- [39] L. Lundberg, A. Soria-Verdugo, D. Pallarès, R. Johansson, H. Thunman, The role of fuel mixing on char conversion in a fluidized bed, *Powder Technol.* 316 (2017) 677–686, <https://doi.org/10.1016/j.powtec.2016.10.060>.
- [40] A. Gómez-Barea, P. Ollero, B. Leckner, Optimization of char and tar conversion in fluidized bed biomass gasifiers, *Fuel* 103 (2013) 42–52, <https://doi.org/10.1016/j.fuel.2011.04.042>.
- [41] H.C. Park, H.S. Choi, The segregation characteristics of char in a fluidized bed with varying column shapes, *Powder Technol.* 246 (2013) 561–571, <https://doi.org/10.1016/j.powtec.2013.06.019>.
- [42] GKD DE | World Wide Weave n.d. <https://www.gkd-group.com/de-de/> (accessed February 6, 2021).
- [43] : magnolithe, feuerfeste Produkte Steine Sande Massen Bauteile Hüttenbedarf Gießereibedarf n.d. [http://www.magnolithe.at/pages/en/firma/fa\\_rohstoffe.htm](http://www.magnolithe.at/pages/en/firma/fa_rohstoffe.htm) (accessed March 2, 2021).
- [44] J. Meng, Z. Zhao, X. Wang, A. Zheng, D. Zhang, Z. Huang, et al., Comparative study on phenol and naphthalene steam reforming over Ni-Fe alloy catalysts supported on olivine synthesized by different methods, *Energy Convers. Manage.* 168 (2018) 60–73, <https://doi.org/10.1016/j.enconman.2018.04.112>.
- [45] M. Jiliang, C. Xiaoping, L. Daoyin, Minimum fluidization velocity of particles with wide size distribution at high temperatures, *Powder Technol.* 235 (2013) 271–278, <https://doi.org/10.1016/j.powtec.2012.10.016>.
- [46] S. Chiba, A.W. Nienow, T. Chiba, H. Kobayashi, Fluidised binary mixtures in which the denser component may be flotsam, *Powder Technol.* 26 (1980) 1–10, [https://doi.org/10.1016/0032-5910\(80\)85001-7](https://doi.org/10.1016/0032-5910(80)85001-7).
- [47] G. Lardier, J. Kaknics, A. Dufour, R. Michel, B. Cluet, O. Authier, et al., Gas and Bed Axial Composition in a Bubbling Fluidized Bed Gasifier: Results with Miscanthus and Olivine, *Energy Fuels* 30 (2016) 8316–8326, <https://doi.org/10.1021/acs.energyfuels.6b01816>.
- [48] Ahrenfeldt J, Vendelbo Foged E, Strand R, Birk Henriksen U. Development and test of a new concept for biomass producer gas engines 2010.
- [49] Jenbacher GE, JENBACHER, G. E. Technical Instruction No.: 1000-0302. Fuel Gas Quality, Special Gases 2009.